DELINEATING DRAWDOWN LAKES AND SALIX ALAXENSIS IN INTERIOR ALASKA USING LANDSAT TM AND MULTITEMPORAL SAR IMAGERY

By

Julieanne Leigh Fogde

RECOMMENDED:

David Verbyla 18 JULY 2001

Advisory Committee Chair

Department Head

APPROVED:

Dean, SALRM

Dean of the Graduate School

Date

DELINEATING DRAWDOWN LAKES AND SALIX ALAXENSIS IN INTERIOR ALASKA USING LANDSAT TM AND MULTITEMPORAL SAR IMAGERY

A

THESIS

Presented to the Faculty
Of the University of Alaska Fairbanks
In Partial Fulfillment of the Requirements
For the Degree of

MASTER OF SCIENCE

By
Julieanne L. Fogde, B.S.

Fairbanks, Alaska

August 2001

ABSTRACT

This study evaluates the effectiveness of multitemporal Synthetic Aperture Radar (SAR) data and Landsat ETM+ imagery to delineate:

1. The locations of drawdown lakes within the Iditarod River drainage.
2. The locations of *Salix alaxensis* along the Innoko River.

Both elements are related in that they constitute critical wildlife habitat, and their occurrence is largely due to seasonal flooding.

Multitemporal, georeferenced Radarsat SAR imagery was used to classify lakes as either drawdown or non-drawdown. This technique yielded an overall classification accuracy of 78%, proving that multitemporal, georeferenced SAR is a good tool for delineating drawdown lakes.

Landsat ETM+ imagery was used to develop three criteria (proximity to turbid water, broadleaf vegetation, and sandbars) to delineate *S. alaxensis*. Areas that met all three of the criteria had an estimated producer's accuracy of 4% for *S. alaxensis,* indicating that this technique is ineffective at delineating *S. alaxensis*.

TABLE OF CONTENTS

LIST OF FIGURES

LIST OF TABLES

ACKNOWLEDGEMENTS

My deepest thanks go to my committee chair, Dr. Dave Verbyla. Dr.Verbyla's patience and guidance have been invaluable. I would also like to thank the U.S. Fish and Wildlife Service, Innoko National Wildlife Refuge (NWR) Biologist Dr. Robert Skinner for providing inspiration and support for the entire project. Funding and field support provided by the Innoko NWR was also greatly appreciated.

Many thanks also go to my committee members Dr. Shusun Li and Dr. William Stringer. And of course, no thesis would be complete without acknowledging the support provided by the unsung heroes of the GIS lab who keep the computers, printers, and programs all in operation and who always seem to know a simpler faster way to make it all work.

CHAPTER 1. INTRODUCTION

1.1 Physical Principles of Remote Sensing

Sabins (1997) defines remote sensing as the science of acquiring, processing and interpreting data regarding the interaction between matter and electromagnetic energy. He further restricts the definition to data acquired by aircraft and satellites. In order to understand why I chose to use multiple sensors for this study it is important to first understand what is meant by electromagnetic energy and how it interacts with matter.

1.1.1 Electromagnetic Radiation

Visible light, heat, and microwaves are all forms of electromagnetic energy. The wave theory states that in a vacuum, all electromagnetic energy propagates at the speed of light (c) in a harmonic, sinusoidal wave pattern with an electric wave perpendicular to the source of propagation, and a magnetic wave with the same wavelength and frequency at right angles to the electric wave (Campbell, 1996). Electromagnetic waves can be described by their wavelength (λ, the distance from the crest of one wave to the crest of the next), their frequency (ν, the number of wave crests passing a giving point in a unit of time) and their polarization[1] (which is the orientation - either vertical or horizontal - of the electric component in an electromagnetic wave) (Figure 1).

Equation 1 (Sabins, 1997) illustrates the relationship between velocity, wavelength and frequency for all forms of electromagnetic energy. The speed of light in a vacuum is essentially constant (~$3x10^8$ m/s) resulting in an inverse relationship between wavelength and frequency. For the purpose of this study, I will use wavelength to describe different forms of electromagnetic energy.

---

[1] Electromagnetic waves can be filtered in such a way that the electric component of the wave is restricted to a single plane perpendicular to the propagation source. Microwave energy used in radar remote sensing can be transmitted and received in either vertical (V) or horizontal (H) polarizations. Four of the most common combinations of polarizations for transmitted and received microwave energy are: HH (horizontal transmit, horizontal receive), HV (horizontal transmit, vertical receive), VH (vertical transmit, horizontal receive), and VV (vertical transmit, vertical receive). Objects that scatter microwave energy and are oriented vertically will scatter more vertically polarized energy than horizontally oriented objects (Waring et al, 1995).

$$c = \lambda\nu \quad (1)$$

The electromagnetic spectrum divides the continuum of electromagnetic energy into regions based on wavelength (Figure 2). The most commonly known regions are those associated with what the human eye can detect, namely blue (0.4-0.5 μm), green (0.5-0.6μm), and red (0.6-0.7 μm). Other regions of the electromagnetic spectrum include the near-infrared region (0.7-100 μm) and the microwave region (0.1-100cm); the area of the spectrum that is used by Radio Detecting and Ranging (radar) systems.

1.1.2 Surface Scattering and Interaction with Materials

Incoming electromagnetic energy that interacts with matter is referred to as incident radiation. Energy that passes through the atmosphere and interacts with materials on the surface of the Earth can be affected in several ways. It can pass directly through the medium (transmitted), altering its velocity if the new medium has a different density (refracted). It can be absorbed, resulting in a heating of the matter, which can then emit the energy as heat. It can be deflected in all directions (scattered) or it can be reflected in one direction (Figure 3).

Gasses such as ozone, water, and carbon dioxide in the Earth's atmosphere absorb energy at specific intervals along the electromagnetic spectrum. These intervals are referred to as absorption bands. The location of absorption bands along the electromagnetic spectrum determines what wavelengths of energy are least useful in a remote sensing system. For example: a satellite with a sensor designed to record ultraviolet radiation reflected from the Earths surface for purposes of vegetation discrimination would be less than ideal because ozone in the Earth's atmosphere absorbs the majority of incoming ultraviolet radiation before it reaches the surface of the Earth.

Once EM energy passes through the atmosphere, interactions between incident radiation and the surface depend largely on two factors: the wavelength of radiation and the nature of the matter that it interacts with. Take, for example, a body of water. The

shorter blue and green wavelengths scatter more than the longer red wavelengths. This type of phenomena – known as Rayleigh scattering – is the reason why the sky is blue. In water, most of the blue, green, red and nearly all of the incoming IR radiation is absorbed within the first few centimeters (Drury, 1998). Since the color of water is determined by volume scattering, deep, clear water appears blue to the human eye. But not all water is deep and clear. Finely textured sediments suspended in water will lower the transmittance of energy through water and shift the surface reflectance towards the longer wavelengths making slightly turbid water appear more green than blue, and extremely turbid water red than green (Campbell, 1996).

Taking the example of the surface reflectance of a body of water one step further, suppose that the wavelength of the incident radiation was approximately 5.4 cm (C-band radar). At this wavelength the microwave radiation is unable to penetrate water. Instead, the water acts as a mirror – or specular reflector – and reflects nearly all of the incident radiation away from the energy source (Waring et al, 1995). In terms of satellite remote sensing this means that very little energy is returned to the sensor, and calm water, regardless of its sediment load, appears very dark. Rough water – a diffuse reflector – will scatter the energy in all directions (Figure 4), resulting in an intermediate intensity signal return. Refer to Sabins (1997) for a further discussion of surface roughness criteria (also called the Rayleigh criterion).

Every type of material has a different spectral response to EM radiation. Materials that are similar, for example birch and aspen trees, share similar spectral responses at the broad-band canopy level. Dissimilar objects such as vegetation and certain rock types (for example, shale) have distinctly different spectral responses in the reflected infrared region of the electromagnetic spectrum. Satellite sensors have been engineered to take advantage of this property. The American Landsat satellites have – among others – sensors sensitive in the 0.76-0.90μm range. These longer wavelengths are useful for discriminating vegetation types and for mapping shorelines.

The Canadian satellite, Radarsat, emits a pulse of microwave energy with a 5.6 cm wavelength. At this wavelength, one of the factors influencing spectral reflectance is

the dielectric constant of the material that the EM radiation encounters. Most natural materials, when dry, have a dielectric constant in the range of 3 to 8. Water has a dielectric constant of about 80 (Weast, 1984). This means that the presence of moisture in soil or vegetation can greatly affect the strength of the radar backscatter.

Each type of sensor (radar and optical) has strengths and weaknesses. Combining the strengths of each sensor yields information about a landscape that a single sensor is not able to do (Nezry et al, 1993; Michelson et al, 2000).

Figure 1. An electromagnetic wave consists of two waves: the electric wave and a magnetic wave at right angles to each other and perpendicular to the source of propagation. (Adapted from Lillesand and Kiefer, 2000)

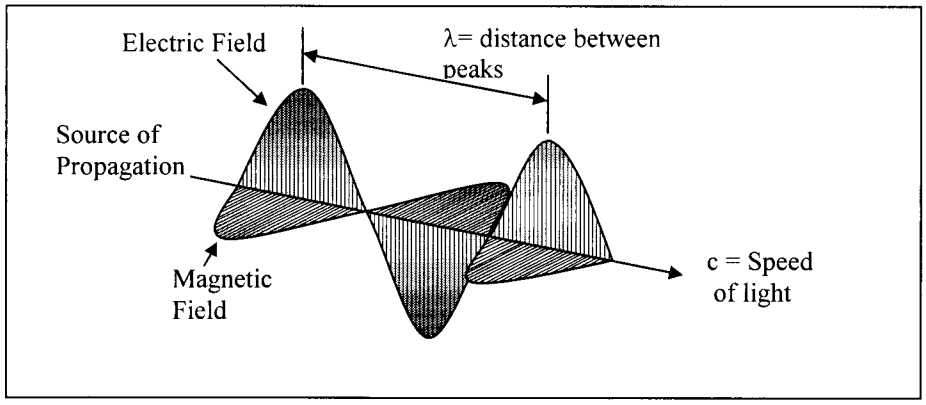

Figure 2.The electromagnetic spectrum. (Adapted from Lillesand and Kiefer, 2000)

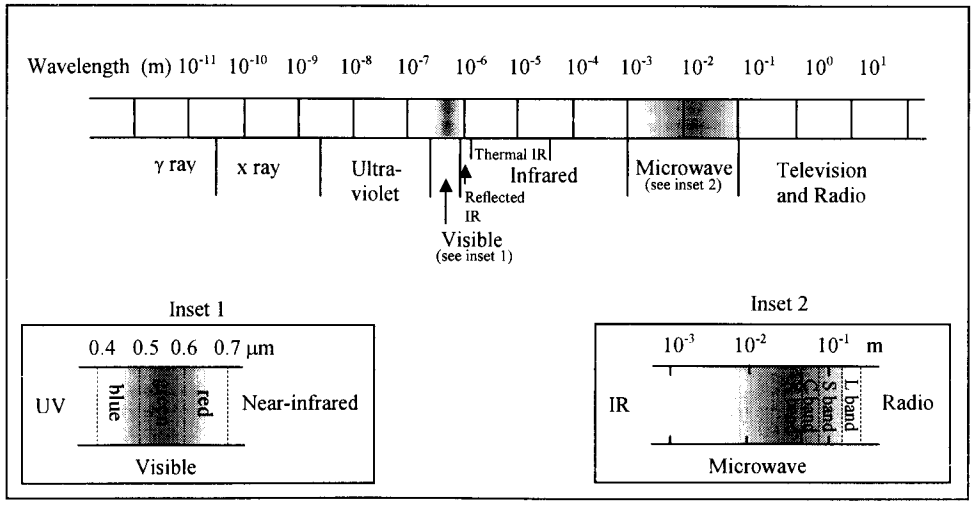

Figure 3. Incident energy can be scattered, reflected, transmitted, or absorbed and re-emitted as heat.

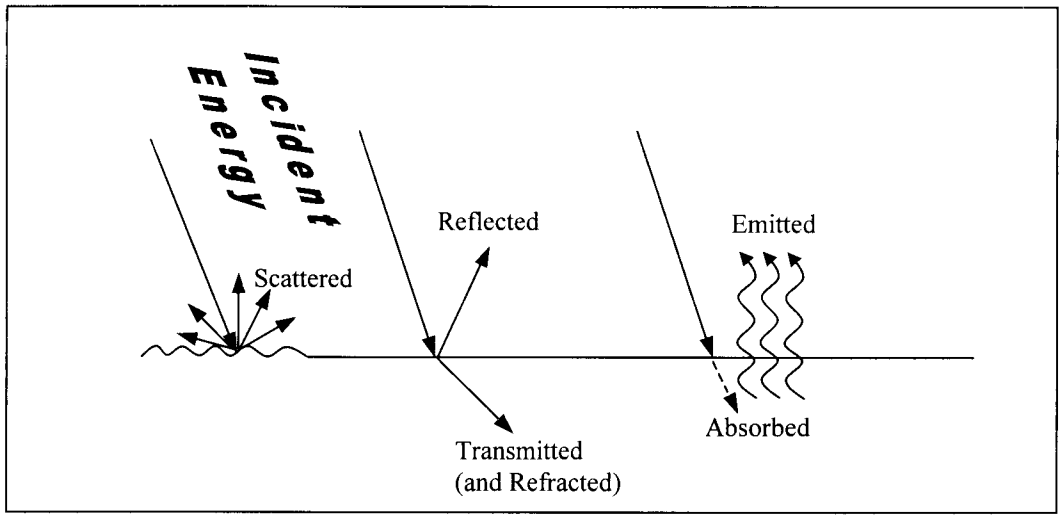

Figure 4. Surface roughness can affect the return intensity of a SAR pulse (Adapted from Sabins, 1997).

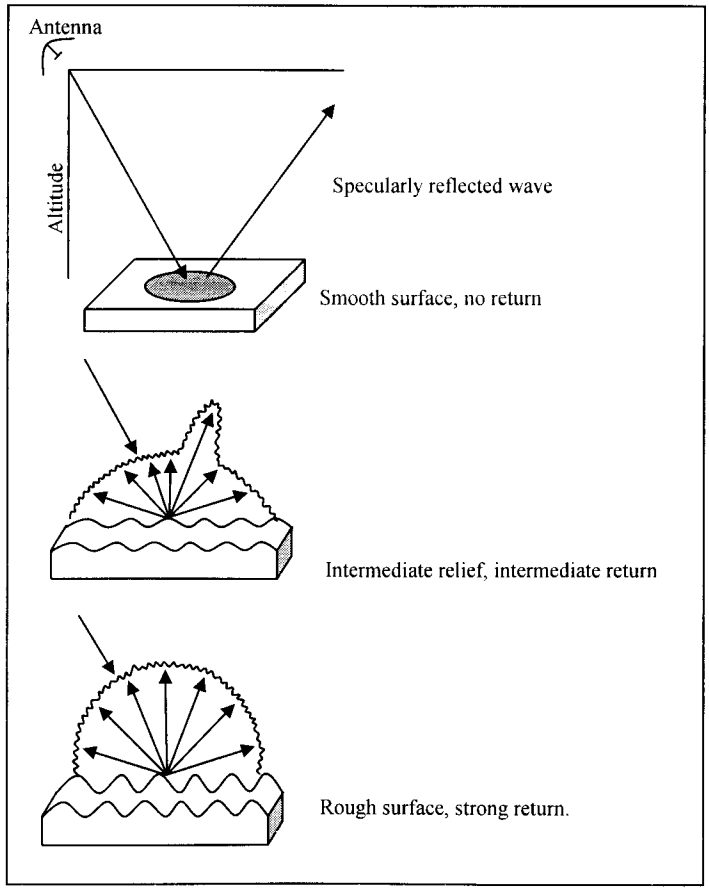

1.2 Sensor Characteristics

The images used in this study were acquired by Landsat satellites 5 and 7, and by the Canadian Radarsat satellite. Refer to Appendix A Tables 6 - 9 for sensor and orbital characteristics.

1.2.1 Optical Sensors

The Landsat satellites carry onboard passive optical sensors. They are designed to detect reflected solar radiation in the visible, reflected IR, and thermal IR regions. (See Appendix A Tables 1 and 2 for sensor specifications.) The Landsat satellites have proven themselves to be useful tool in a wide variety of fields including geology, land use planning oceanography, forestry, environmental monitoring, agriculture and others (Lillesand and Kiefer, 2000). The relatively large area covered per scene (183x170 km) combined with a ground resolution cell size of 30x30 meters makes using Landsat images more practical than low altitude aerial photographs for applications that cover large areas. Landsat TM and ETM+ are also sensitive to a wider range of EM energy than that typically sensed by the film used to acquire low altitude aerial photographs[2].

Each area of the EM spectrum yields information about the landscape that can aid in the development of a land cover classification. The shorter wavelengths (0.45-0.52μm, Landsat TM band 1) are more useful for shallow water bathymetry, while the slightly longer wavelengths (0.63-0.69μm and 0.76-0.90, Landsat TM bands 3 and 4) are more useful for assessing plant vigor. The reflected IR portion of the spectrum (0.76-0.90μm, Landsat band 4) yields information about biomass, soil moisture, and plant vigor and is good for delineating water bodies. An ideal combination of Landsat TM or TM+ bands for visual discrimination of vegetation would use a visible band (bands 1, 2 or 3) with a near IR band (band 4) and a mid-IR band (bands 5 or 7)(NOAA, 1984; Jenson and Cowen, 1999).

---

[2] Color IR film is sensitive to energy ranging from 0.3 – 0.9 μm, while Landsat ETM+ is sensitive to energy ranging from 0.45 – 2.35μm and 10.4 – 12.5μm (Sabins, 1997).

1.2.2 Active Microwave Sensors

RADARSAT, JERS-1, and ERS-2 satellites are all Synthetic Aperture Radars[3] (SAR). SAR is an active sensor, which means it illuminates the surface of the earth with a pulse of energy in the microwave region of the electromagnetic spectrum, and then records the returned echo. (See Appendix A Tables 8 and 9 for sensor specifications.) In this manner it works much like a camera with a flash.

SAR systems have several distinct advantages over passive optical systems like Landsat TM. Because SAR is an active sensor it is able to image the earth regardless of the amount of daylight present. SAR systems also operate in a portion of the electromagnetic spectrum that is not strongly affected by atmospheric gasses or conditions such as cloud cover, smoke, or haze. This all-weather capability makes using SAR ideal for areas frequently obscured by clouds, such as the arctic, sub-arctic and tropics.

Interpreting SAR imagery is not as straightforward as interpreting imagery acquired in the more familiar visible portion of the EM spectrum. Microwave reflections from the surface of the Earth result in images that are in no way similar to images of the same area from optical sensors. SAR images are influenced by the geometry, composition and moisture content of surfaces as well as the look angle, look direction, polarization, and wavelength of the sensor.

The variables that influence the strength of the returned microwave signal are given in the RADAR equation (Equation 2)(Campbell, 1996):

---

[3] In radar remote sensing, azimuth resolution is controlled by the length of the antenna, the slant range distance, and the wavelength of the transmitted pulse (Equation 3) (Sabins, 1997).

$$R_a = \frac{0.7 \cdot S \cdot \lambda}{D} \qquad (3)$$

R_a is the azimuth resolution, S is the slant range distance, λ is the wavelength of the transmitted pulse, and D is the length of the antenna (also called the aperture). From this equation we can calculate an azimuth resolution of 10 meters for a sensor with a 7-meter long antenna, 1 cm wavelength, and a slant range distance of 10 km. If we wanted to achieve the same azimuth resolution from a sensor on a satellite (S = 700, and λ = 1 cm), our antenna would be 490 m long! Synthetic Aperture Radar overcomes this problem by using sensor motion to 'synthesize' a much longer antenna.

$$P_r = \frac{\sigma G^2 P_t \lambda^2}{(4\pi)^3 R^4} \quad (2)$$

P_t is transmitted energy, P_r is the energy received from the surface, R is the distance from the target to the sensor, λ is the wavelength of transmitted energy, and G is a measure of the sensor's ability to focus the transmitted energy. The backscatter coefficient (σ) is a quantitative measure of the energy returned to the sensor and is the only variable controlled by the characteristics of the surface material.

Dielectric constant, surface roughness (discussed in section 1.1.2) and microtopography are among the landscape elements that influence σ (Campbell, 1996). The presence of moisture increases the dielectric constant of most materials. As moisture content increases microwaves tend to scatter from the surface more readily than with drier materials. Plants usually have high moisture contents and are therefore good reflectors of microwave energy. Shorter wavelengths (2-6 cm) are generally thought of as ideal for remote sensing of the vegetation canopy. As the canopy moisture content increases, so does σ, resulting in a brighter image signature. It should be noted that metal objects also have a high dielectric constant and will therefore yield a very bright radar signature.

Topography has a significant effect on the strength of the backscatter return. Variations in the local incidence angle[4] (Figure 5) result in high backscatter returns from slopes facing the sensor and very little return from slopes facing away from the sensor. As a general rule, for local incidence angles between 0-30°, σ is dominated by topographic slope. Incidence angles between 30° and 70° are dominated by surface roughness, and for angles greater than 70°, radar shadows dominate[5] (Figure 6) (Lillesand and Kiefer, 2000).

---

[4] Local incidence angle is defined as the angle formed between a line normal to the target and another connecting the antenna and the target.

[5] In areas with steep topography the tops of mountains are detected before their bases. The result is that mountains and hills appear slanted or laid over towards the sensor. A radar shadow is a dark signature on a radar image that represents no signal return. It extends in the far range direction from an object that intercepts a radar wave.

Other examples of difficulties associated with interpreting SAR images include the same target (for example, water) having a different backscatter response depending on wind conditions. Another example is wet versus dry snow. Because of the difference in dielectric constant between dry and wet snow, the same object – snow – will have a different backscatter response. Another example is in urban environments where some – but not all – buildings serve as corner reflectors, while other areas may have minimal backscatter. With optical sensors, the spectral response of water versus urban versus snow is consistent in many spectral regions.

Radar images also contain a form of granular noise referred to as speckle. Speckle results from the constructive and destructive interference of waves that are reflected from many elementary scatters (Kasischke et al, 1997). The presence of speckle complicates image interpretation and reduces the effectiveness of image classification (Lee and Jurkevich, 1989).

The most common method of reducing the presence of speckle involves the use of a filter kernel[6]. Early efforts to suppress speckle used a mean or median filter, however because speckle is a multiplicative, random process (Lewis et al, 1998), adaptive filters, such as the Lee or Frost filters, have proven to be better suited to suppressing speckle while simultaneously preserving the sharpness of point, line and edge features (Lee et al, 1994).

For a more technical review of imaging radar systems, SAR image interpretation, and applications refer to Henderson and Lewis (1998).

[6] A filter kernel is a two-dimensional array of pixels with an odd number of rows and columns. The central pixel is modified based on the surrounding pixel values. Once a new value for the center pixel has been calculated, the filter moves one pixel to the right and recalculates the center pixel's value. This procedure continues until the right margin of the filter kernel meets the right margin of the image, at which point the filter kernel moves to the left margin of the next row. This process is repeated for all rows of the image (Sabins, 1997).

Figure 5. An example of how topography affects local incidence angle.

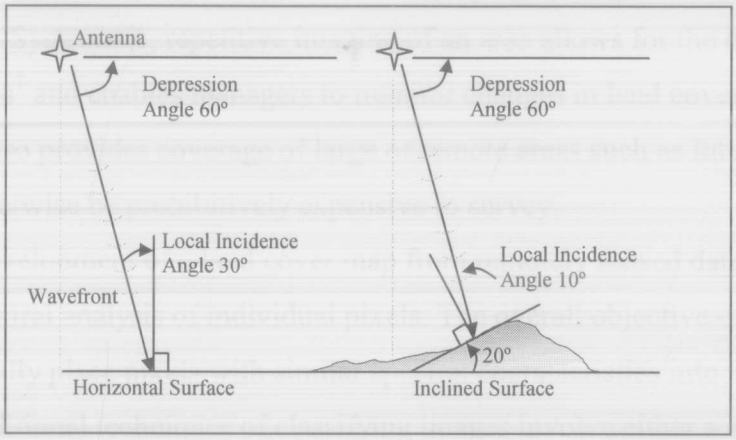

Figure 6. Effect of terrain on SAR imagery (Adapted from Raney, 1998).

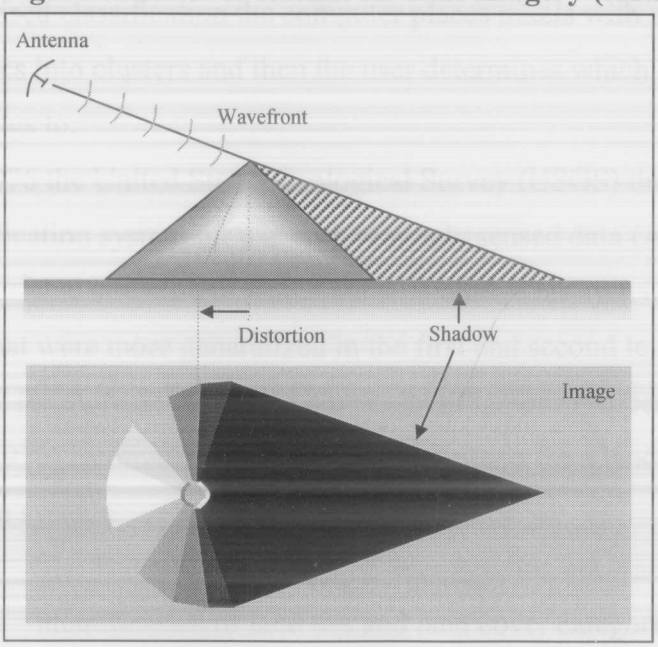

1.3 Literature Review

Satellite imagery of the Earth offers land use managers a unique view of the landscape. Systematic, repetitive imaging of an area allows for the development of land cover maps[7] and enables managers to monitor changes in land cover over time. Satellite imagery also provides coverage of large or remote areas such as Interior Alaska, which would otherwise be prohibitively expensive to survey.

Development of a land cover map from remotely sensed data typically begins with a spectral analysis of individual pixels. The overall objective of which is to automatically place pixels with similar spectral characteristics into the same category or class. Traditional techniques of classifying images involve either a supervised or unsupervised method. In a supervised classification the user provides a computer with spectral response examples of known land cover types (also called training areas), which the computer then uses as a guideline for classifying the remaining areas of the image. In an unsupervised classification the computer places pixels with similar spectral characteristics into clusters and then the user determines which land cover class each cluster belongs to.

In 1976 the United States Geological Survey (USGS) developed a land use/land cover classification system for use with remotely sensed data (Anderson et al, 1976), the basic concepts and structure of which are still valid. This system classified land into categories that were more generalized in the first and second levels, but left room at the higher levels for more detailed land cover classifications (Appendix B, Table 10). Anderson (1976) recommended the following criteria for a land use / land cover classification system:

> "1. The minimum level of interpretation accuracy in the identification of land use and land cover categories from remote sensor data should be at least 85%.

---

[7] Land cover is defined as the types of materials (buildings, rocks, lakes, forests, etc.) that are found on the surface. Land use refers to the economic function of a piece of land (recreational park, housing development, agricultural, etc.).

2. The accuracy of interpretation for the several categories should be about equal.
3. Repeatable or repetitive results should be obtainable from one interpreter to another and from one time of sensing to another.
4. The classification system should be applicable over extensive areas.
5. The categorization should permit vegetation and other types of land cover to be used as surrogates for activity.
6. The classification system should be suitable for use with remote sensor data obtained at different times of the year.
7. Effective use of subcategories that can be obtained from ground surveys of from the use of larger scale or enhanced remote sensor data should be possible.
8. Aggregation of categories must be possible.
9. Comparison with future land use data should be possible.
10. Multiple uses of land should be recognized when possible."

The use of multiple sources of data to improve land cover classifications has been well documented. Information regarding elevation, slope, aspect, and climate as well as multi-temporal and multi-source imagery have all been used with varying degrees of success to improve the accuracy of land cover classifications (Table 1).

Schriever and Congalton (1995) hypothesized that seasonal variability in spectral reflectance (as a result of leaf biomass, water content, and chlorophyll absorption) could be used as an aid to improve land cover classification of some Northeastern forest types. They speculated that spectral variability due to leaf biomass, water content, and chlorophyll absorption would be the greatest during autumn senescence of Northeastern

hardwoods. They found that Landsat TM imagery acquired in October was significantly better at classifying their 9 forest cover types (74% overall accuracy, 99% confidence level) than similar imagery acquired in September. Additionally, imagery acquired during or shortly after bud break in May yielded better results (69% overall accuracy, 95% confidence level) than the September image. Schriever and Congalton made no attempt in their study to improve the accuracy of their classification by combining data from different dates.

In a similar study by Wolter et al (1995) multi-temporal Landsat TM and MSS imagery was used to discriminate 22 forested land cover classes with an overall accuracy of 83.2%. The key to the high level of estimated accuracy in their study lies in the fact that the authors were able to acquire cloud-free imagery of the study site during times when different species of trees showed the highest level of phenological variability. They used the spectral variability inherent in different species of trees at different times of year to improve their classification. An example of this is to use an image acquired during the winter to differentiate tamarack (a *deciduous* needle-bearing tree) from other needle-bearing trees.

Multi-temporal radar imagery is particularly well suited to map the temporal and spatial properties of seasonal wetland inundation. Radar backscatter from areas with a vegetated canopy is markedly different than areas with standing water under a vegetated canopy (Milne et al, 2000; Pope et al, 1997; Hess et al, 1995). Radar sensors do not possess the optical sensors inability to penetrate cloud cover.

Wang et al (1998) compared multi-date ERS-1 imagery to single date Landsat TM imagery for wetland classification. They found that multi date ERS-1 imagery yielded better results than single date imagery, but that there was no significant improvement if more than five dates were used. The best multi-date combination resulted in an overall classification accuracy of 85%. Although, single date, multispectral Landsat TM imagery still proved to be better than ERS-1 imagery for wetland classification (overall accuracy of 97% for the 6 land cover classes identified in the study). However, in the instance that

cloud free Landsat TM data cannot be obtained, multi-date ERS-1 imagery could yield satisfactory results.

Milne et al (2000), Pope et al (1997), and Hess et al (1995) each presented similar papers regarding the utility of SAR in distinguishing vegetation classes and mapping wetland inundation patterns. Milne et al (2000) mapped the drying phase of the tropical wetlands of the Kakadu National Park, Northern Territory, Australia with multi-temporal RADARSAT SAR imagery. Pope et al (1997) tested the utility of multi-temporal SIR-C radar imagery to detect the extent of flooding under 11 different wetland land cover categories in the Yucatan Peninsula. They found C band HV imagery to be most useful for detecting inundation under each of the 11 land cover classes. Hess et al (1995) also used SIR-C radar imagery in a supervised land cover classification (5 classes: water, clearing, aquatic macrophyte, forest and non-flooded forest) of a portion of the Amazon floodplain.

In some situations, multi-temporal imagery (aimed at catching changes in plant phenology) is not able to improve land cover classifications. In mountainous regions lower sun angles in the fall, winter and spring create shadows in areas that would otherwise be in full sunlight. Geometric distortions such as layover and shadowing of SAR imagery in mountainous areas makes using radar inappropriate for land cover classifications (Kasischke et al, 1997).

Cibula and Nyquist (1987) were able to successfully use elevation and climatological data to improve a land cover classification in the mountainous Olympic National Park. Using Landsat MSS data from acquired in July and aerial photographs taken several years prior to the study, Cibula and Nyquist were able to increase the number of land cover classes (from 9 to 21) while maintaining a high overall level of accuracy (91.7%). They accomplished this by partitioning the study area into 7 unique watersheds, and the subjecting the original 9 land cover classes in each watershed to Boolean decision tests that incorporated elevation, slope, aspect, and precipitation/climate regimes.

The accuracy of a land cover classification can be affected by spectral confusion among similar land cover types and by the presence of mixed pixels[8](Ioka and Koda, 1986). Janssen et al (1990) was able to minimize the influence of mixed pixels in their land cover classification of two agricultural regions in the Netherlands. Using aerial photographs they were able to define 'objects' or areas that only one land cover class was expected to occur in and apply these boundaries to a Landsat TM derived land cover map. Pixels in each object were reassigned to a new land cover class based on the majority land cover class for that object. It was assumed that the majority of pixels located within an object were correctly classified. Overall accuracy increased from 72% to 84% for the 6 land cover classes defined in the Ulvenhout region and from 76% to 96% for the 7 land cover classes defined in the Biddinghuizen region.

[8] Mixed pixels result from the combination of the spectral reflectances of different objects and are typically found at the boundary between two or more land cover classes.

Table 1. Examples of recent attempts to improve land cover classifications.

Ecosystem	Purpose	Data source	Number of classes	Overall Accuracy	Reference
Northeastern U.S. forest	Forest cover	Single date Landsat TM	9 forest classes	74%	Schriever and Congalton, 1995
Northern Great Lakes	Forest cover	Multi-temporal Landsat TM & MSS	22 forest classes	83.2%	Wolter et al (1995)
Temperate rain forest	Land cover	Single date Landsat MSS	21 vegetation classes	91.7%	Cibula and Nyquist (1987)
Temperate lowland	Land cover	Single date Landsat TM	6 veg. classes in Ulvenhout region 7 veg. classes in Biddinghuizen region	84% in Ulvenhout 96% in Biddinghuizen	Janssen et al (1990)
Northern wetland	Land cover	Multi-temporal ERS-1	6 vegetation classes (3 of which were wetland)	85%	Wang et al, 1998

CHAPTER 2. STUDY AREA AND OBJECTIVES

2.1 Ecology of Innoko National Wildlife Refuge

In 1980 Congress enacted the Alaska National Interest Lands Conservation Act (ANILCA), Public Law 96-487, effectively creating over 100 million acres of new refuges, national parks, conservation areas, recreation areas, forests, monuments, and wild and scenic rivers in the state of Alaska. According to section 101a, the purpose of ANILCA is to "preserve for the benefit, use, education and inspiration of present and future generations certain lands and waters in the State of Alaska that contain nationally significant natural, scenic, historic, archeological, geological, scientific, wilderness, cultural, recreational, and wildlife values..." The land encompassed by the Innoko National Wildlife Refuge (NWR) was selected because of its unique gold rush history, raptor, fish and furbearer populations, and waterfowl and moose habitat.

The boundaries of the Innoko NWR now encompass approximately 3.8 million acres boreal forest and lowland muskeg bogs dotted with hundred of wetlands, lakes and ponds. Located approximately 300 miles northwest of Anchorage, Alaska (Figure 7) the Innoko NWR is dominated by the meandering, sediment laden, slow moving waters of the Yukon, Innoko, Iditarod, Dishna, and Yetna Rivers (Alt, 1983), which form the oxbows and sloughs (Figure 8) favored by many waterfowl.

The vegetation on the refuge is a mixture between the vegetation types common to the boreal forests of Interior Alaska and the shrub/tundra lands of western and northern Alaska. A land cover classification based on Landsat imagery estimated that wetland vegetation classes dominate nearly half of the land on the refuge. Forested classes cover approximately one fourth of the refuge (Figure 9; Appendix C, Table 11) (USFWS, 1987; Talbot, 1987).

The well drained soils along the riparian corridor of the Innoko river support large stands of white spruce (*Picea glauca*), paper birch (*Betula papyrifera*), alder (*Alnus tenufolia*), and willow thickets (*Salix alaxensis* and *Salix pulchra*) (Figure 8). Black spruce muskeg typically forms outside of the river corridor in poorly drained soils underlain by permafrost with black spruce (*Picea mariana)*, dwarf birch (*Betula nana*),

alder (*Alnus crispa*), and tamarack (*Larix laricina*) forming the dominant vegetation species (Figures 10 and 11).

The climate is continental sub-arctic with an average temperature of 6.5° F in the winter and 50° F during the summer, with annual average precipitation near 18" including 81" of snow (Selkregg, 1976).

The large moose and waterfowl populations on the refuge can be attributed to the yearly flooding and draw down regimes of the lakes. Spring floods due to snow melt and breakup, and summer flooding due to rainfall removes or buries organic layers, adds nutrients, and deposits a layer of silt, all of which enhance the growth of willows – a primary food source for moose (Figures 12 and 13). Flooding also recharges the more than 26,000 lakes on the Refuge and gives draw down lakes[9] the characteristics that are favored by many dabbling ducks and geese. Draw down promotes annual seed crops, abundant invertebrate populations, and emergent vegetation (Swanson, 1988).

[9] A draw down lake is defined as a lake with a connection to a river during normal water level conditions. Small changes in water level result in significant changes in surface area exposed. Waterfowl use is determined by the phase of the draw down cycle (Swanson, 1988).

Figure 7. Map of the study area used for the delineation of draw down lakes (Iditarod River area) and Salix alaxensis (Innoko River area).

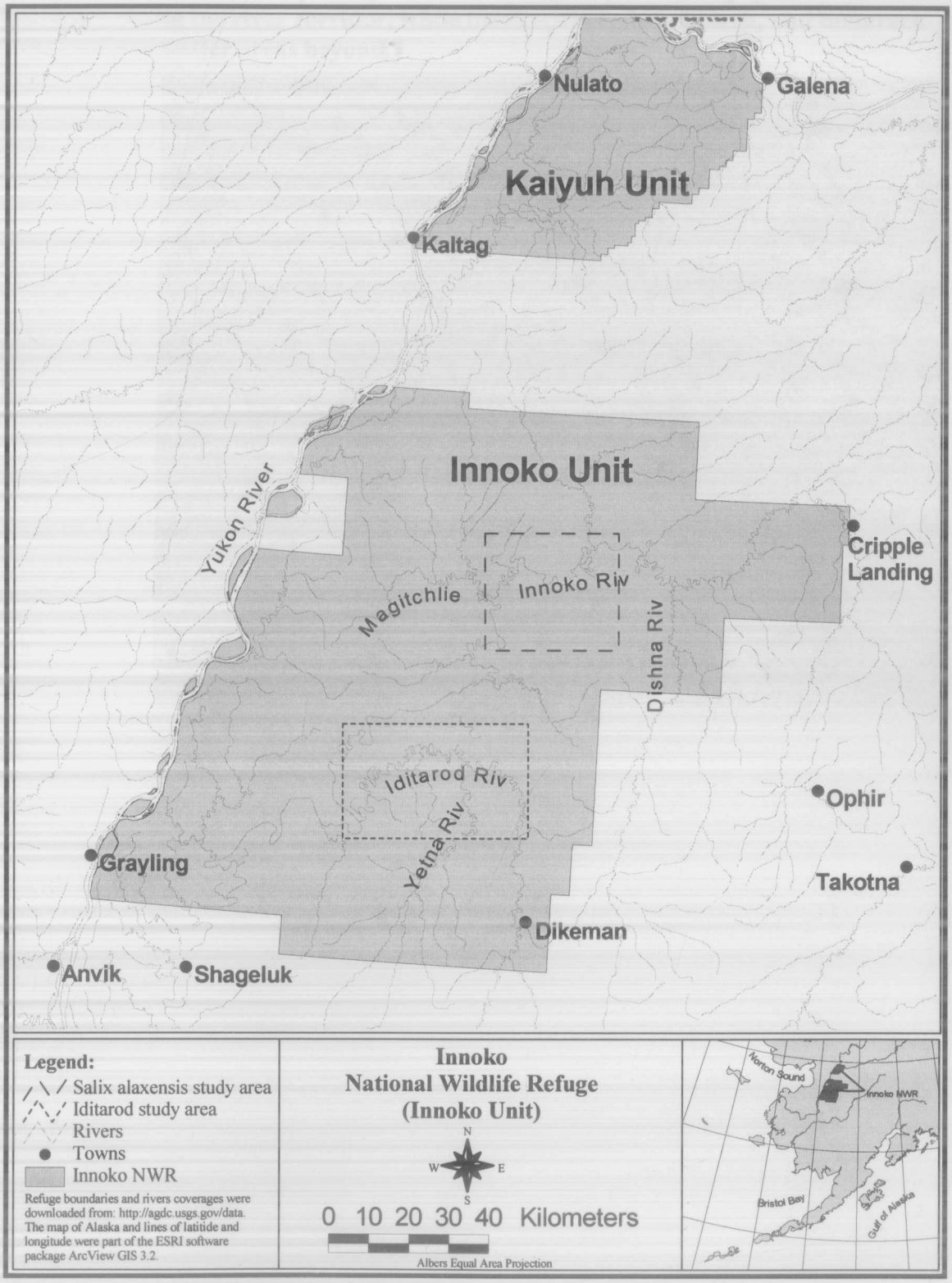

Figure 8. The slow moving Innoko River creates the numerous oxbow lakes and sloughs that are favored by many waterfowl. White spruce and paper birch are dominant along the river corridor, while black spruce, dwarf birch, and tamarack dominate the wetter areas beyond.

Figure 9. Land cover classification of the Innoko NWR (Talbot and Markon, 1987).

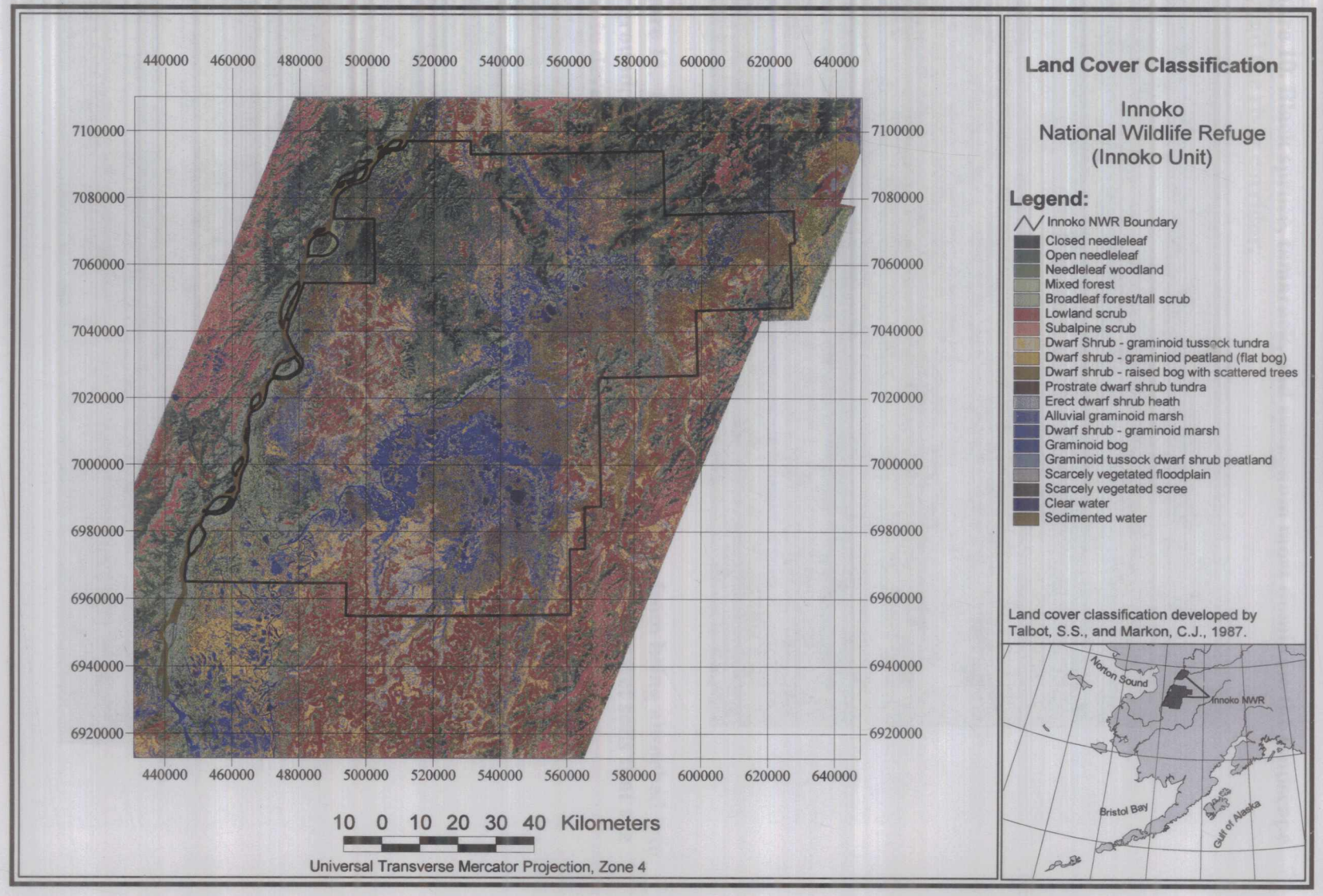

Figure 10. Black spruce, tamarack, and sphagnum moss dominate the landscape beyond the river corridor.

Figure 11. Permafrost prevents rain and melting snows from being absorbed into the ground, resulting floating sphagnum moss mats above very wet soils that are slow to develop.

Figure 12. Summer flooding deposits nutrients, which in turn enhance the growth of willows.

Figure 13. Spring flooding from snowmelt and break up replenishes nutrients to the thousands of lakes located on the Innoko NWR.

2.2 Rational and Applications

In the past, habitat surveys on the Innoko NWR have been limited by the inability of field crews to access some of the more remote areas of the Innoko NWR and the shear size of the area to be covered. The use of satellite imagery provides land use managers with a method of acquiring multi-spectral data over large remote areas. Currently the majority of ecosystem maps generated from satellite imagery are based on the Level I and II classified units described in Anderson's (1976) paper.

It is important to remember that a classification scheme must first be relevant to potential users. A Level II land cover classification may not provide the user with the level of detail required for a specific study. In these cases alternate methods for improving the land cover classification must be sought out. This can include increasing the spectral or temporal resolution of the images used, or integrating ancillary data (such as elevation, slope, aspect, and latitude) with remote sensor data.

In regards to describing forest cover types Eyre (1980) recommends to "...give recognition to the ecological factors that helped create the (forest) types and will continue to influence their development." This philosophy can also be applied to improving land cover classifications. On the Innoko NWR annual flooding influences the extent and distribution of certain species of willows as well as altering the limnological characteristics of lakes within the zone of flooding.

SAR lends itself well to wetland detection and delineating the extent of surface flooding (Wang et al, 1998; Hess et al, 1995; Pope et at 1997; and Milne et al 2000). The all weather capability of SAR and its sensitivity to moisture provides users with the ability to monitor variations in surface conditions on a regular interval. Maps generated from this type of information can then be used as data layers to aid in the design of stratified surveys or to examine the relationship between remotely sensed data and moose or waterfowl distributions.

2.3 Study Objectives and Assumptions

This study evaluates the effectiveness of multi-temporal SAR data in combination with Landsat TM imagery to delineate:

1. The locations of lakes within the Iditarod River drainage that have a connection to a river during normal water level conditions.
2. The locations of *Salix alaxensis* along the Innoko River corridor.

Both elements are related in that they constitute critical habitat for several different species of wildlife on the Innoko National Wildlife Refuge (NWR), and that their occurrence is largely due to seasonal flooding.

Of the 33 species of willow occurring in Alaska, 8 grow large enough to be classified as trees (Viereck and Little, 1972). Proper identification is complicated by within species variability and the fact that many species of willow hybridize. On a strictly spectral basis it is very difficult - if not impossible - to separate closely related species of willow. However, if regional distribution, growth form, and habitat preference are taken into consideration it becomes easier to narrow the number of possible species. One of the key assumptions in this study is that *Salix alaxensis* is the only species of willow growing in large stands on the banks of the Innoko River and that it does not occur anywhere outside of the river corridor. This assumption was based on aerial surveys and ground observations, however, as stated earlier, distinguishing closely related or hybridized species of willows can be difficult.

The second assumption in this study is that no new draw down lakes were created between the time the imagery was acquired and the time the ground truth was collected. Over the course of a season it is possible for a beaver to damn the mouth of a lake or for debris from flooding to lodge in the outlet and block the natural flow of water. It is also assumed that all obstructions that could affect the flow of water from a lake outlet were clearly visible from a helicopter or airplane.

An effort has been made to ensure that all geographic data used in this study were registered to each other as closely as possible. In most instances, the estimated positional error is less than 15 meters.

2.4 Study Area

Salix alaxensis occurs in valleys throughout most of Alaska and is a preferred browse species of moose (*Alces alces*)(Viereck and Little, 1972). Skinner et al (1996) determined that *Salix alaxensis* and *Salix pulchra* comprise more than 90% of the winter forage for moose in the Innoko River drainage. This estimate agrees with Risenhoover's (1989) estimate of a moose's winter diet in Interior Alaska consisting >94% of four different willow species including *S. alaxensis* and *S. planifolia* (also called *S. pulchra*). On the Innoko NWR *S. alaxensis* grows primarily along the sandbars that form along the inside bends of the river (Figure 14). The delineation of *Salix alaxensis* will be limited to the section of the Innoko River riparian corridor shown in Figure 7.

Innoko NWR's extensive wetlands have been deemed to be one of the most important nesting and breeding sites for many species of waterfowl including: white front and Canada geese, tundra and trumpeter swans, widgeon, pintail, and scaup. Selkregg (1976) reported that more than a million ducks and an estimated 450,000 geese migrate from the Innoko-Koyukuk[10] area each year. During the summer of 2000 an estimated 20,000 Canada and White front geese were recorded on the Innoko NWR alone, the majority of which were concentrated in the southern portion of the Innoko NWR near the Iditarod River (Figure 15) (B. Platte, pers. comm.). The detection of draw down lakes will focus on the Iditarod River drainage (Figure 7).

[10] The Koyukuk NWR is approximately 200 km north-northeast of the Innoko NWR

Figure 14. *S. alaxensis* is an early successional species that dominates sandbars shortly after grasses such as *Calamagrostis canadensis* become established.

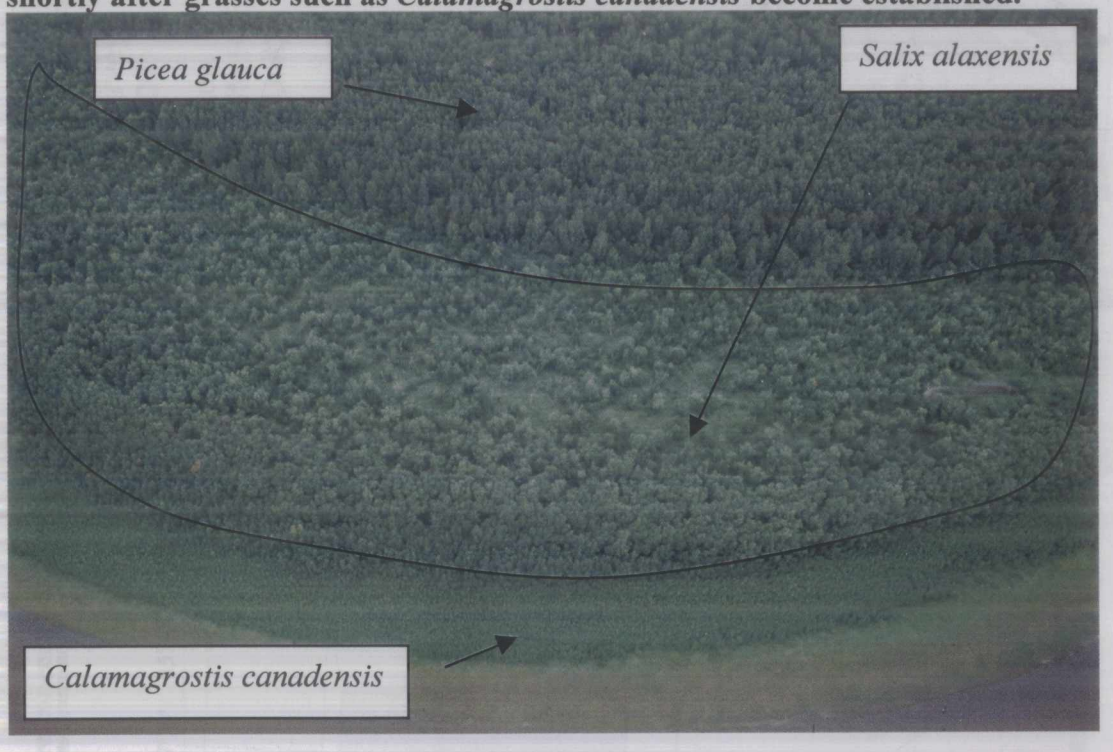

Figure 15. The majority of waterfowl found on the Innoko NWR are concentrated around the Iditarod River drainage.

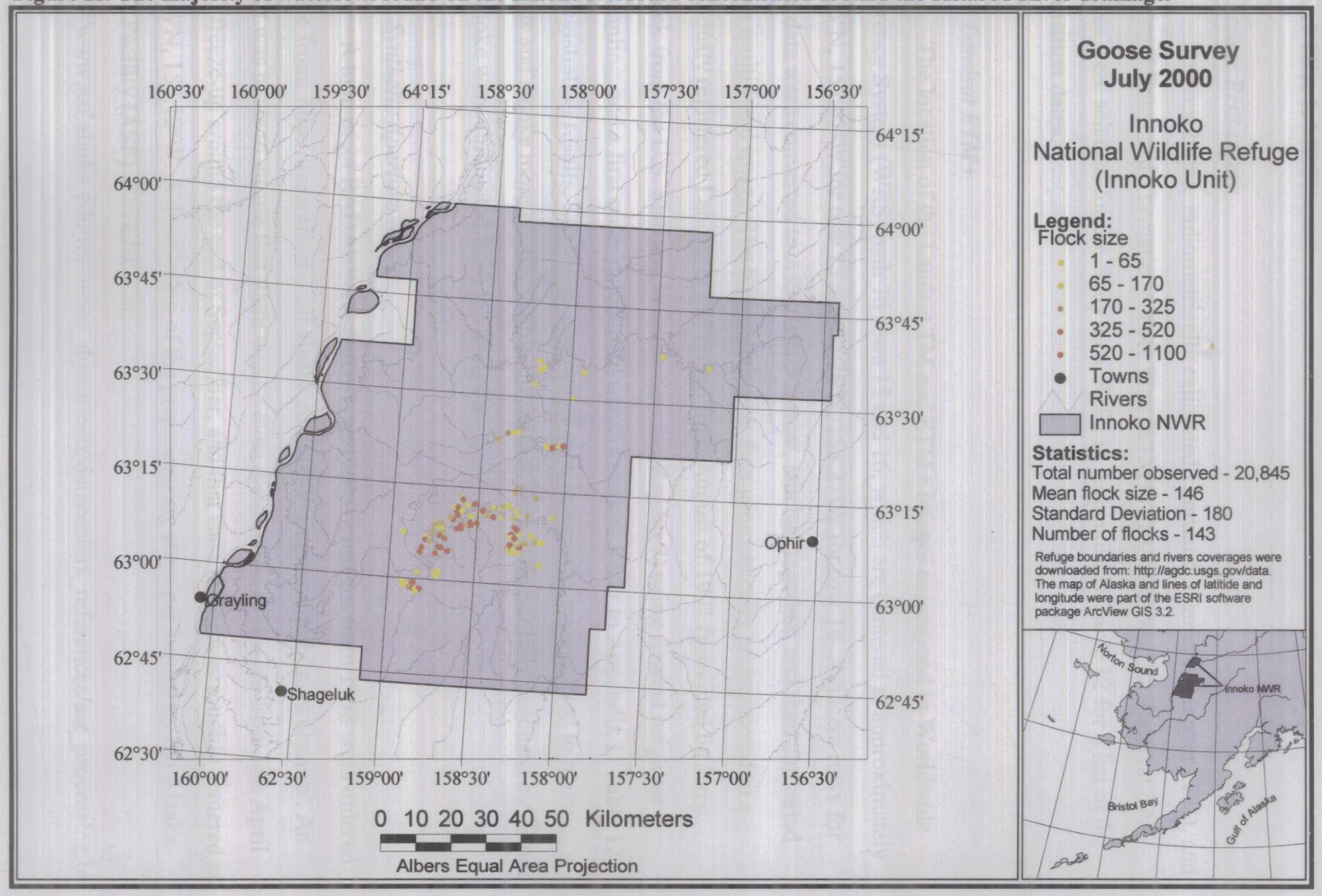

CHAPTER 3. METHODS

3.1 Image Processing

Full resolution, radiometrically calibrated Landsat 5 Thematic Mapper (TM), and Landsat 7 Enhanced Thematic Mapper Plus (ETM+) images as well as Radarsat SAR images were selected for the study area. Refer to Appendix D Table 12 for a list of the acquisition dates.

3.1.1 Landsat ETM+

The location of the Landsat TM and ETM+ images correspond to Worldwide Reference System (WRS) path 76 rows 15 and 16, which are centered at approximately 64.25°N, 157.01°W for row 15 and 62.75°N, 158.27°W for row 16. Adjacent rows for each date were converted to ARC/GRID format, stitched together, and then converted into a multi-band image. The ETM+ data was then geometrically co-registered to a previously registered Landsat 5 TM image from August of 1991 (provided by Jerry Minick from the U.S. Fish and Wildlife Service, Region 7) using nearest neighbor resampling, and a first order polynomial transformation. Refer to Appendix D Table 12 for registration results. The visual contrast of each image was manipulated to make clouds and smoke more readily visible. Areas that were even partially obscured by clouds or smoke were eliminated from the analysis.

3.1.2 Synthetic Aperture Radar

A total of 24 RADARSAT, JERS-1, and ERS-2 images from 1998 were ordered online from: http://imswelcome.asf.alaska.edu:8000/~imswww/pub/imswelcome/. An effort was made to ensure that there was an even distribution of images from late April until freeze-up around the end of September, and that each image was roughly centered at 63.54°N, 158.12°W. A description of the preprocessing steps performed by the Alaska SAR Facility (ASF) is available at: http://www.asf.alaska.edu/reference_documents/datacenters_references/sar_processing.html.

Each SAR image was calibrated and geocoded using the Alaska SAR Facility's "calibrate" and "sarautoreg" routines. The calibrate routine rescales sigma-naught to values between 0 and 255 so they can be displayed as an image. The sarautoreg routine uses information contained within the header file and user-defined projection information to place the image in geographic space. These programs and detailed documentation are available from http://www.asf.edu.

Registering SAR images that contain complex topography require methods that make use of a digital elevation models to correct for foreshortening and layover. Ranson and Sun (1994) found that in relatively flat areas (maximum change in elevation of 0.68%) a simple first order linear interpolation yielded much better registration results than a third order polynomial interpolation. The maximum change in elevation within the study site on the Innoko NWR is less than 0.68% making corrections for foreshortening and layover unnecessary.

The image processing program ENVI was used to geometrically register each SAR image to the 1991 Landsat image using nearest neighbor resampling and a first order polynomial transformation. The extreme remoteness of the study site and the lack of any permanent, recognizable features made identifying ground control points difficult. As a result, control point selection was limited to areas that had relatively stable, permanent bodies of water.

Each image was filtered using ENVI's 3x3 Lee filter. Lee and Jurkevich (1994) reported that a Lee filter preserves the mean value of a SAR image while simultaneously reducing speckle and maintaining edge sharpness. As a final step, each image was converted into ARC/INFO Grid format. Images acquired on the same day, in the same orbital path, and from the same satellite were stitched together in the same manner as the Landsat TM images.

3.2 Validation Data

Ground control and ground truth locations were recorded during the summers of 1998 and 2000 using a Precision Lightweight GPS Receiver (PLGR). These GPS units

are capable of determining location to within about 5 meters using the military's encrypted "P-code."

3.2.1 Ground Control

To assess the registration accuracy of the Landsat 5 TM image a Cessna 185 on floats, a riverboat and a PLGR were used to collect 95 ground control points at locations where creeks and streams joined the Yukon and Innoko Rivers (Refer to Appendix E Figure 25 and Table 13 for information regarding the location of ground control points). Points were recorded only when the plane or boat had come to a full stop as close to the landscape feature as possible. An effort was made to ensure that the points were as widely located across the refuge as possible. 39 of the original 95 ground control points were readily located on the imagery. The mean distance of the ground control points to their corresponding location on the imagery was 12.18 meters ($s = 14.41$, $n = 39$), which is within acceptable limits.

3.2.2 Ground Truth

To assess the accuracy of the predicted locations of *S. alaxensis* and draw down lakes it is important to first have accurate knowledge of where these features occur on the landscape as well as where they don't occur. This kind of information is called ground truth or reference data.

3.2.2.1 Draw Down Lakes

In order for a lake to be termed 'draw down' its outlet had to be free from obstructions such as beaver dams and wide enough to allow the passage of a small boat or canoe at normal water level conditions. Using 1:63,360 scale topographic maps, aerial photographs, a handheld GPS, and a float plane or helicopter, the locations of draw down lakes and non draw down lakes were recorded in the field during the summer of 1998 and 2000. Refer to Appendix E Figure 26 and Tables 14 and 15 for a list of reference data

coordinates of the center point of each draw down and non draw down lake and a map of their geographical distribution.

3.2.2.2 Salix alaxensis

Field crews, each equipped with a PLGR, collected ground truth of 63 stands of *S. alaxensis* along the Innoko River corridor. The location of individual plants and plants that as a group were no more than about 5 meters wide were noted, but not recorded. Each field crew walked the perimeter of a qualifying stand of *S. alaxensis* while recording their location with the PLGR every five to ten meters. *S. alaxensis* occurred most frequently in areas of recent alluvial deposition (Figure 16). Stands of *S. alaxensis* are generally crescent-shaped with the width of 60 meters (n = 15, s = 25) at their widest point and a length of 904 meters (n = 15, s = 596). Refer to Appendix E Figure 27 and Table 16 for a list of reference data coordinates of *S. alaxensis* stands and a map of their geographical distribution.

Figure 16. Willows generally occur in areas of recent alluvial deposition (Adapted from Pielou, 1994).

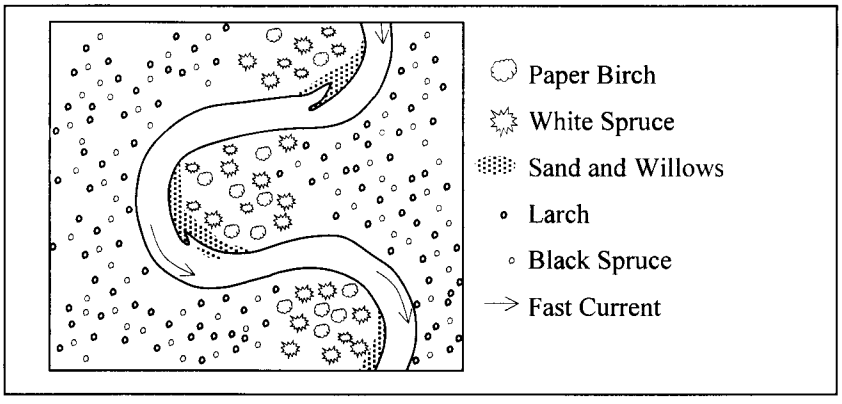

3.3 Classification

3.3.1 Draw Down Lakes

Daily stream flow data collected from the Iditarod River and some of its tributaries indicated lower than average stream flow between mid-June and early July of 1998 (M. Linne, pers. comm.) (Figure 17). Based on the stream flow data and visual interpretation of the SAR images acquired between the dates of April 1, 1998 and September 30, 1998 I selected one Radarsat image from the end of this period (July 6, 1998) to represent the 'draw down' water stage, and one Radarsat image from September 15 to represent an 'average' water level.

Figure 17. Combined average daily stream flow of the Iditarod, Yetna and Little Yetna Rivers for the period between April 1, 1998 and September 30,1998.

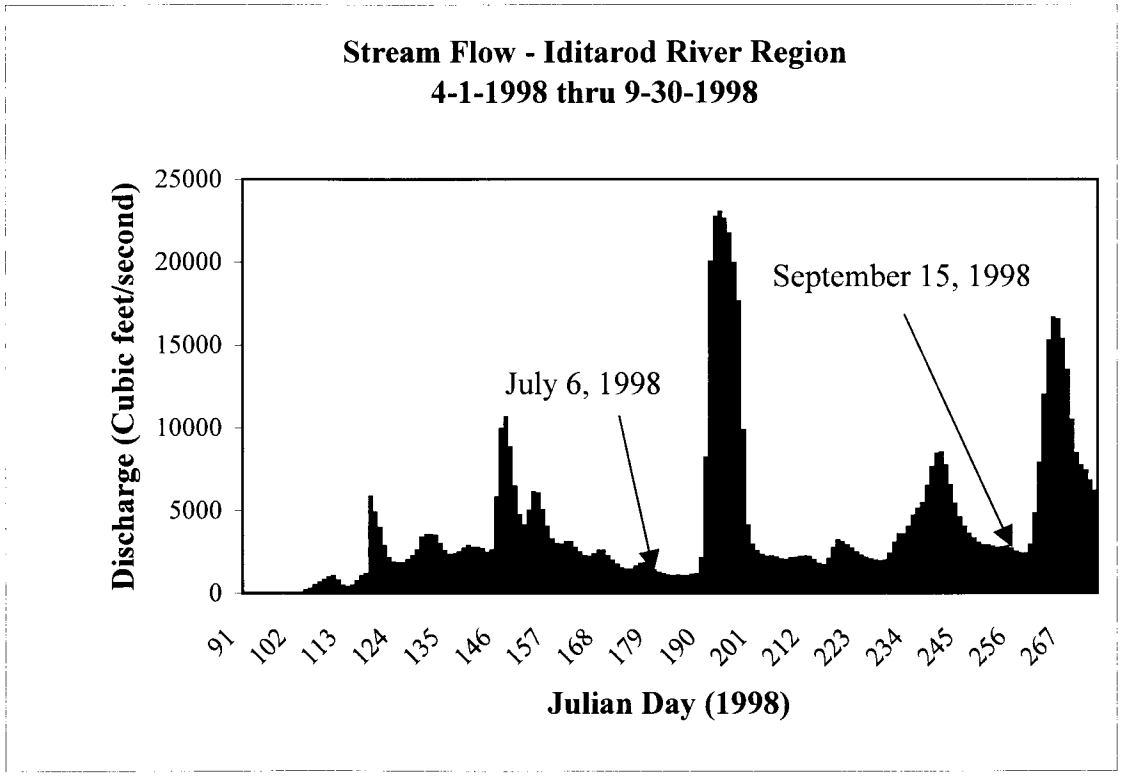

Visual interpretation of the imagery indicated that pixels below a threshold of 70 were generally representative of water. Based on this information, pixels below a threshold of 70 in each image were classified as water. Each contiguous group of pixels

(classified as 'water') from the September 15th image was assigned a unique identifying number. Groups with a total area of less than 1 hectare were eliminated. There were several reasons for this: 1) White front and Canada geese that molt in the Iditarod River drainage generally prefer lakes larger than 8 hectares (Ely and Dzubin, 1994). 2) Very little ground truth was available for lakes smaller than 2 hectares. This lack of information at the lower size range made it difficult to develop a model that predicts the locations of all draw down lakes. While it is important not to neglect the environmental significance of ponds smaller than 1 hectare, for the purposes of this study it was impractical.

The outer boundary of each group of pixels from the September 15th image that was larger than 1 hectare was then expanded by 60 meters. The 'expanded' group of pixels was then used to assign the same unique number to the lake during low water levels (July 6th image). By doing this I was able to compare the change in surface area without worrying about the slight positional error associated with each image. This technique is illustrated in Figure 19.

A simple random sample without replacement of draw down lakes and non-draw down lakes was used to develop criteria for classifying lakes from the imagery into one of the two categories. For each lake in the sample population percent change in area[11] was calculated (Table 2 and Appendix F Tables 17 and 18). Figure 18 graphically illustrates the difference in percent change between draw down lakes and non-draw down lakes. In general, most draw down lakes lost more than 15% of their surface area.

Table 2. Statisics for sample populations of draw down lakes and non draw down lakes.

	Mean % Change	Sample Standard Deviation	Number of Samples
Non Draw Down Lakes	-1.41	15.75	13
Draw Down Lakes	-44.55	37.50	20

[11] percent change = area at low water / area at high water * 100 - 100

Figure 18. Most draw down lakes experience a negative change in surface area of more than 15%, while non draw down lakes rarely show a negative change in their surface area.

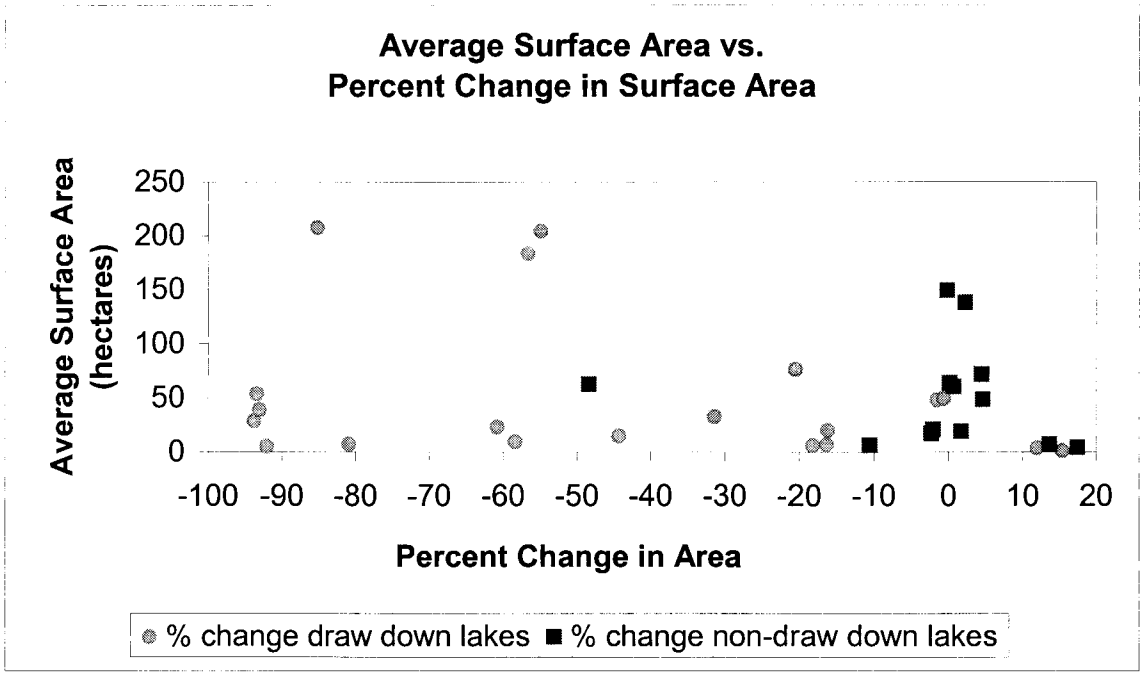

The one non-draw down lake outlier (-48% change in surface area from September 15th to July 6th) is an old oxbow lake that was once part of the Innoko River. At the time of my aerial survey of the area the lake did not appear to have a clear connection to the river. It is unlikely that the lake underwent a change that would have changed its classification from non-draw down to draw down between the time the imagery was acquired and the ground truth collected since the two were done within weeks of each other. It is more likely that an error was made during the aerial survey of the lake. What looked like an obstruction from the air might not actually have affected the flow of water from the river to the lake.

Figure 19 Diagram of method used to reduce the influence of positional error in the detection of draw down lakes.

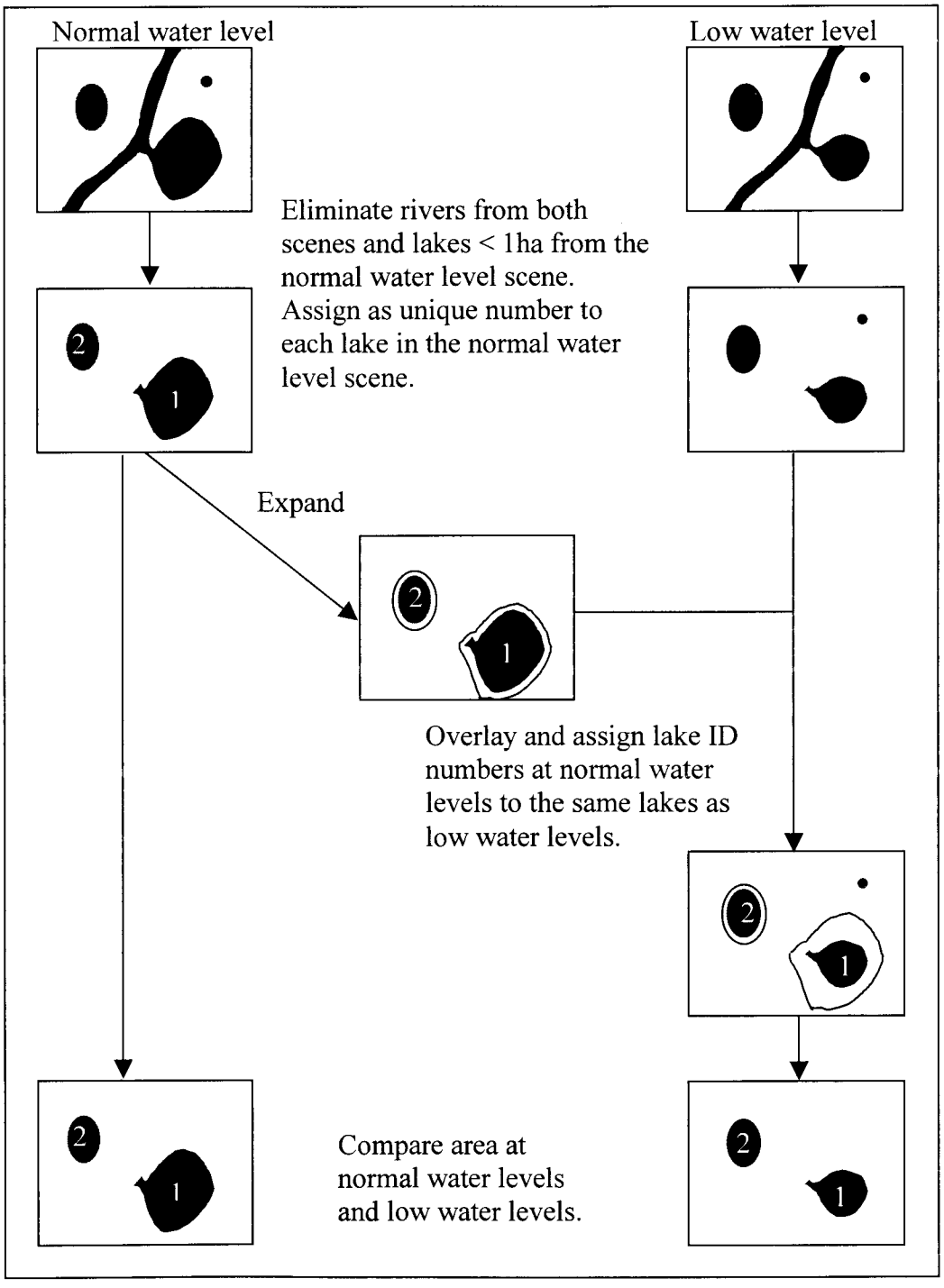

3.3.2 Salix alaxensis

The *S. alaxensis* that occurs in the Innoko River study area is a deciduous shrub or small tree (6-9 meters in height and 10-18 cm in diameter)(Viereck and Little, 1972) that tends to grow along sandbars in slender crescent-shaped patches that are generally no more than 60 meters at their widest and taper down to only a few meters in width near the end. This pattern was used to develop a set of criteria for delineating *S. alaxensis* (Figure 20).

All areas that consisted of turbid water were manually digitized from a Landsat 7 ETM+ image from June 30, 1999. The turbid water polygons were buffered by 120 meters and then converted into a grid to match the satellite image pixel size (30 meter pixels). The 120 meter buffer was selected based on the average maximum width of a random selection of stands of S. alaxensis. It was also intended to allow for positional error introduced by the GPS receiver and in the registration process of the Landsat 7 image.

S. alaxensis forms a very narrow boundary (generally less than two or three 30 x 30 meter pixels) between the water (and sand) of the river and the early successional deciduous forests of the land. This means that in most cases a stand of S. alaxensis will be represented mostly if not entirely by mixed pixels. Using color infrared aerial photos of the study area as a reference it was determined that for the ETM+ near-infrared band[12] image, pixels above a threshold of 111 represented broadleaf vegetation. Pixels that met this threshold requirement were selected and buffered by 30 meters (one pixel) in an effort to reduce the influence of mixed boundary pixels.

Sandbars are evident in the June 30, 1999 Landsat 7 ETM+ image (Figure 21). Within the 120 meter buffer of the river, pixels above a threshold of 46 in band 3 were found to be representative of sandbars. Groups of more than 6 contiguous pixels that met this threshold were selected and buffered by one pixel (30 meters).

The GIS themes that resulted from the three criteria (proximity to sandbars, turbid water, and broadleaf vegetation) were overlaid. Areas that met all three of the criteria

[12] Broadleaf vegetation is highly reflective in the near-infrared portion of the electromagnetic spectrum (Sabins, 1996). This corresponds to Landsat ETM+ band 4.

were expected to have a higher likelihood of supporting S. alaxensis than areas that met only one or two of the criteria (Figure 20). The river itself and the area beyond the buffered river corridor were not included in the accuracy assessment.

Figure 20. Flowchart outlining the process used to develop the criteria for delineating Salix alaxensis.

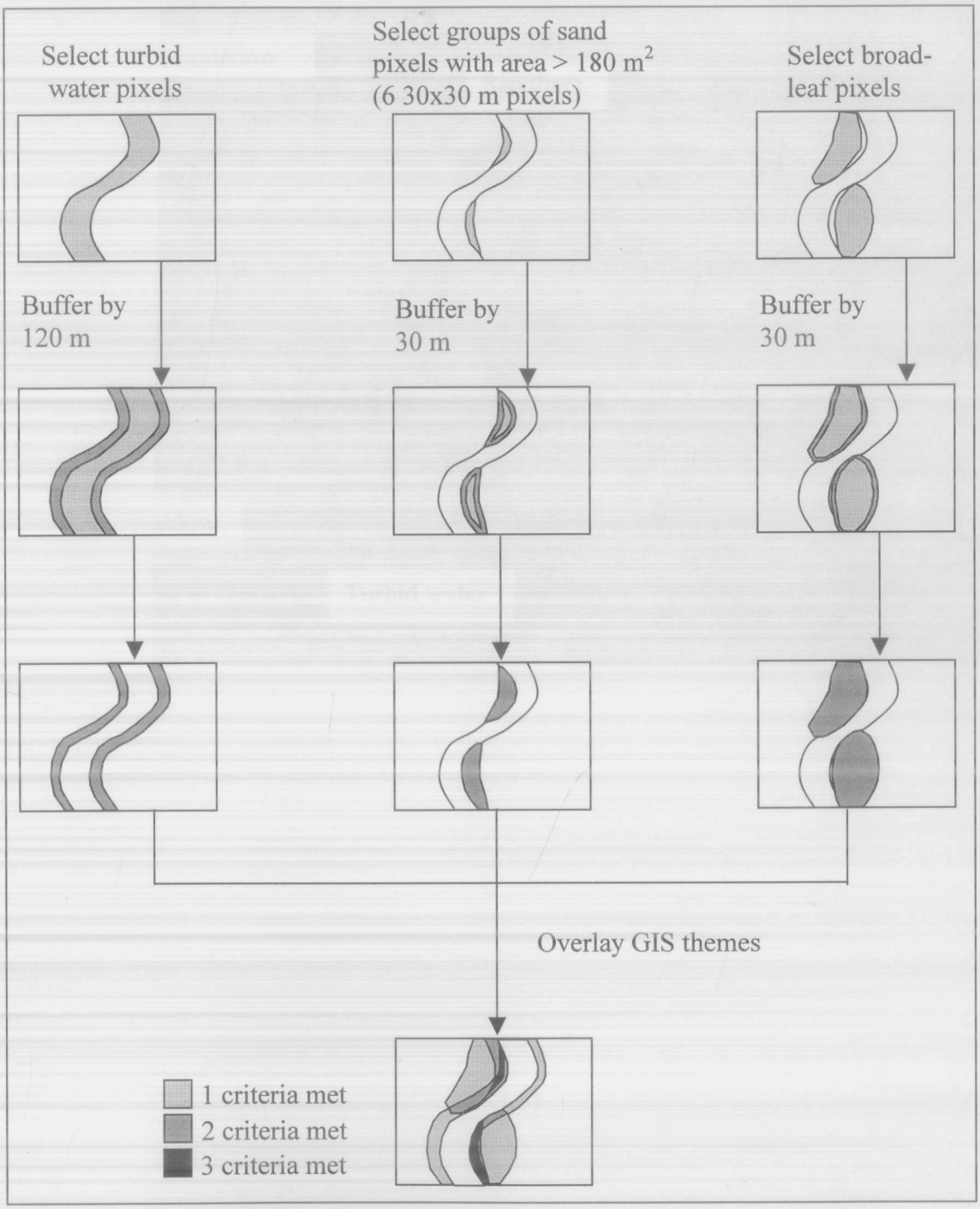

Figure 21. Sandbars appear as light blue patches adjacent to the river on the inside bends. Notice that open grassy meadows also share a similar spectral response, but that they are generally further from the river.

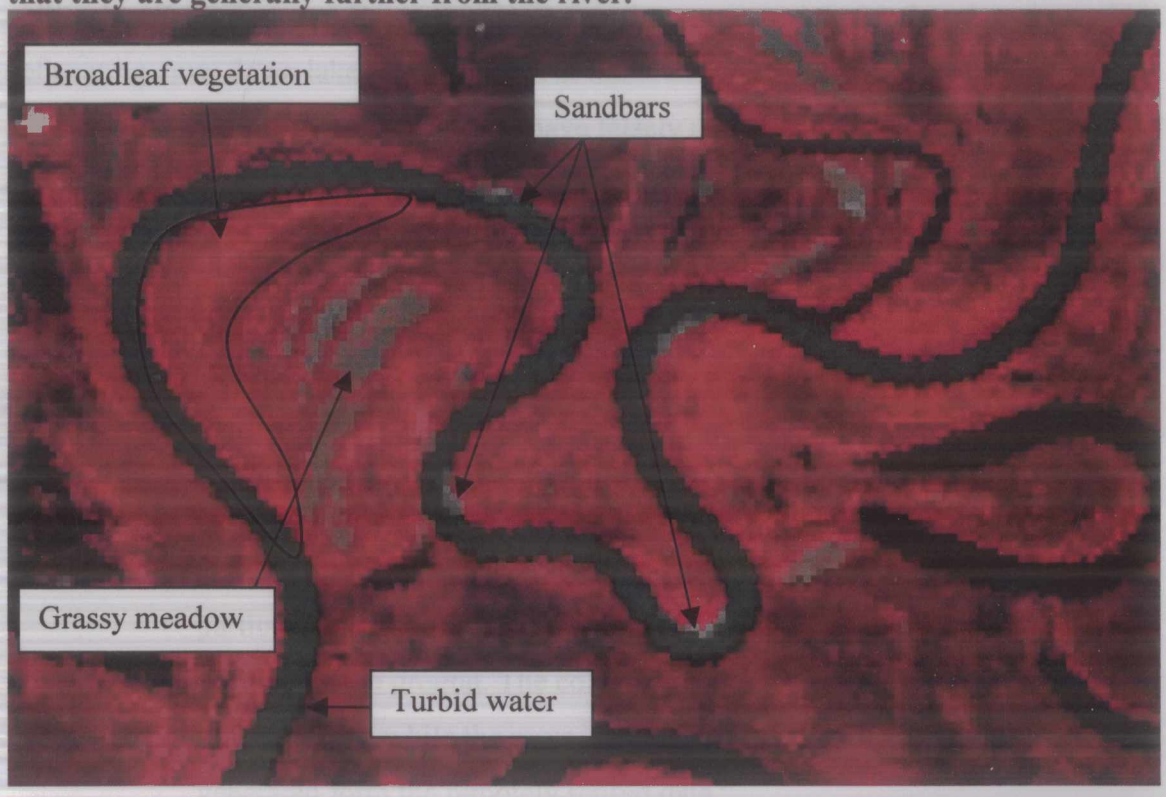

3.4 Accuracy Assessment

Accuracy assessments for the classifications in this study follow the methods outlined in Congalton and Green (1998). Points that were used to develop the criteria for delineating draw down lakes and stands of *S. alaxensis* were excluded from the accuracy assessment. Including these areas would have falsely increased the accuracy of the classification because locations used in the development of the classification model have a greater probability of being correctly classified (Verbyla, 1995).

The most widely used method to quantify errors or estimate the accuracy of a classified image is the error matrix (Skidmore, 1999; Congalton and Green, 1998; Lillesand and Kiefer, 2000). Congalton (1991) describes the error matrix as:

> "...a square array of numbers set out in rows and columns which express the number of sample units (i.e., pixels, clusters of pixels, or polygons) assigned to a particular category relative to the actual category as verified on the ground. The columns represent the reference data while the rows indicate the classification generated form the remotely sensed data."

Overall accuracy is calculated by dividing the total number of correctly classified pixels by the sum of the total number of pixels tested. Producer's accuracy (an estimate of errors of omission) is calculated by dividing the number of correctly classified units in an individual category by the number of training pixels used for that category (the total for that category's column). User's accuracy (an estimate of the errors of commission) is calculated by dividing the total number of correctly classified pixels by the sum number of pixels that were classified into that category (the row total for that category).

Estimates of accuracy of a classification from an error matrix can be misleading. Mere random chance can sometimes yield better results than the original classification. The Kappa analysis is a statistical method used to determine if a classification is better than one generated by random chance. Congalton and Green (1998) conceptually define the Kappa statistic ($\hat{K}$) as:

$$\hat{K} = \frac{observed\ accuracy - chance\ agreement}{1 - chance\ agreement}$$

$\hat{K}$ is a measure of how well a classification agrees with ground truth data. As observed accuracy approaches 1 and chance agreement approaches 0, $\hat{K}$ approaches 1. $\hat{K}$ can range in value from –1 (when chance agreement is large) to +1 but since there is generally a positive relationship between a the classification of remotely sensed image and the reference data, $\hat{K}$ generally ranges from 0 to 1. For example, a $\hat{K}$ value of 0.80 for a classification indicates that an observed classification is 80% better than one resulting from chance. A $\hat{K}$ value close to 0 indicates that a classification is no better than one resulting from random chance.[13]

[13] Equation 4 can be used to compute $\hat{K}$ (Bishop et al, 1975):

$$\hat{K} = \frac{N\sum_{i=1}^{r} x_{ii} - \sum_{i=1}^{r}(x_{i+} \cdot x_{+i})}{N^2 - \sum_{i=1}^{r}(x_{i+} \cdot x_{+i})} \qquad (4)$$

where
r is the number of rows
x_{ii} is the total number of observations for row i, column I
x_{i+} is the number of samples classified into row i,
x_{+i} is the number of samples classified into column i
N is the total number of observations

CHAPTER 4. RESULTS AND DISCUSSION

4.1 Results

4.1.1 Draw Down Lakes

A total of 63 lakes were divided into two categories: draw down and non draw down. Lakes with a negative change in surface area of more than 15% from July 6, 1998 to September 15, 1998 were grouped into the 'draw down' category and the remaining lakes were placed in the 'non draw down' category. This resulted in an estimated producer's accuracy of 80% and an estimated user's accuracy of 88% for draw down lakes. Non draw down lakes had an estimated producer's accuracy of 74% and an estimated user's accuracy of 61%. The estimated overall accuracy was 78% with a $\hat{K}$ of 0.502 (Table 3). Refer to Appendix G, Table 19 for the data used to generate the error matrix shown in Table 3.

Table 3. Error matrix resulting from classification of lakes.

	Training Set Data (Known Cover Types)		
	Draw Down	Not Draw Down	Row Total
Classification Data			
Draw Down	35	5	40
Not Draw Down	9	14	23
Column Total	44	19	
	Producer's Accuracy	**User's Accuracy**	
Draw Down	35/44 = 0.80	35/40 = 0.88	
Not Draw Down	14/19 = 0.74	14/23 = 0.61	
Overall Accuracy = (35+14)/63 = 0.78			
$\hat{K}$ = 0.502			

4.1.2 Salix alaxensis

An estimated user's accuracy of 17% and an estimated producer's accuracy of 4% for *S. alaxensis* resulted in areas where all three of the criteria were met (proximity to turbid water, broadleaf vegetation, and sandbars)(Table 4). Areas that met two of the three criteria had an estimated user's accuracy of 9% and an estimated producer's accuracy of 100% for *S. alaxensis* (Table 5). In both cases $\hat{K}$ values are close to 0, indicating that the classification of Salix alaxensis in this study is no better than one generated by random chance.

While an estimated producer's accuracy of 100% seems good, in this case it simply indicates that 100% of the areas of known *S. alaxensis* were within 120 meters of turbid water and within 30 meters of broadleaf vegetation. The User's Accuracy describes how well the classification was at placing only *S. alaxensis* into the *S. alaxensis* category (errors of commission). In this case only an estimated 9% of the area classified as *S. alaxensis* really was *S. alaxensis*. The remaining 91% consists primarily of a mixture of bluejoint grass (*Calamagrostis canadensis*), rose (*Rosa acicularis*), and birch (*Betula papyrifera*).

An error matrix is not presented for areas that met only one of the criteria because aerial and ground surveys indicated that nearly all S. alaxensis was located within 120 meters of the river.

Table 4. Error matrix resulting from the use of three criteria to delineate *S. alaxensis*.

	Training Set Data (Known Cover Types)		
	S. alaxensis	Not *S. alaxensis*	Row Total
Classification Data			
S. alaxensis	97	488	585
Not *S. alaxensis*	2244	28048	30292
Column Total	2341	28536	
	Producer's Accuracy	**User's Accuracy**	
S. alaxensis	97 / 2,341 = 0.04	97 / 585 = 0.17	
Not *S. alaxensis*	28,048 / 28,563=0.98	28,048 / 30,292 = 0.93	
Overall Accuracy = (97 + 28,048) / 30,877 = 0.91			
$\hat{K}$ = 0.037			

Table 5. Error matrix resulting from the use of two criteria to delineate *S. alaxensis*.

	Training Set Data (Known Cover Types)		
	S. alaxensis	Not *S. alaxensis*	Row Total
Classification Data			
S. alaxensis	2341	23709	26050
Not *S. alaxensis*	7	4820	4827
Column Total	2348	28529	
	Producer's Accuracy	**User's Accuracy**	
S. alaxensis	2341/2348 = 1.00	2341/26050 = 0.09	
Not *S. alaxensis*	4820/28529 = 0.17	4820/4827 = 1.00	
Overall Accuracy = (2341 + 4820) / 30877 = 0.23			
$\hat{K}$ = 0.030			

4.2 Discussion

Overlaying multidate, georeferenced SAR imagery in order to use the pattern of water recession as a method of improving the classification of water bodies on the Innoko NWR proved to be a useful technique. While using the ecological factors that influence the growth of *S. alaxensis* as a way to distinguish a stands of *S. alaxensis* from the surrounding vegetation was ineffective.

4.2.1 Draw Down Lakes

Probably the most important factor that contributed to the success of the detection of draw down lakes is the ease with which SAR can be used to detect surface water (the reason for this is described in section 1.1.2). The boundaries between lakes and the surrounding vegetation are quite clear on images that have been acquired on relatively calm days and a simple thresholding[14] technique can be used to delineate the water bodies. SAR's unique all-weather capability make obtaining multitemporal images is relatively easy. This is especially useful for tracking changes in water levels during times when the study site is obscured by the very same clouds that are providing the rainfall that is causing the water levels to rise. Additionally, because many of the draw down lakes are shallow with muddy, gently sloping shores a small change in water level results in a large change in surface area, and large changes are usually easier to detect than small changes.

Minimization of the influence of positional error in the imagery contributed significantly to the overall success of the draw down lake detection. This minimization was accomplished in several ways. First, ground truth involved simply observing a lake at average water levels and determining if it had an unobstructed connection to the river. Any location recorded with a GPS near the center of the lake would be accurate enough to locate the same lake on the imagery, and since the lakes used in this study were larger than 1 hectare, the positional error of the GPS unit was not an issue. The second method

[14] Thresholding is an image processing technique used to segment an image into two classes based on a single analyst defined gray level value.

that was used to reduce positional error involved the way in which the same unique identifying number was assigned to each lake at normal and low water level conditions (illustrated in Chapter 3, Figure 19).

It is clear from the results that SAR is useful for tracking the patterns of water recession (or inundation). A good illustration of this is shown in Figure 22. Figure 22 is a composite of three Radarsat images acquired on: July 6, 1998; August 23, 1998; and September 15, 1998, displayed as red, green and blue, respectively. For an area to be red it has to have relatively high radar backscatter values in the July 6th image (the image selected to display shades of red) but low values (such as would be associated with smooth water) in the August and September images (the images selected to display blue and green). What this means is that areas that changed from dry to wet between July and September (i.e. the parts of the landscape the experience some sort of inundation due to rainfall or rising river levels) appear red.

Shallow lakes (<61 cm deep) provide important waterfowl habitat (Hudson, 1983). SAR is not able to detect lake depth during the summer months when lakes are ice-free. One of the primary factors that influences radar backscatter is dielectric constant[15] (which is generally dependent on moisture content[16]). Surfaces with high moisture contents tend to strongly reflect incident radar energy. Stated simply: Radar waves do not penetrate more than a few millimeters into liquid water and therefore cannot sense depth or turbidity[17]. However, optical sensors with sensitivity to energy in the blue region of the EM spectrum are able to penetrate water and are therefore useful for summertime shallow bathymetry surveys. This makes them useful for discriminating important waterfowl habitat areas based on lake depth or turbidity. However, studies have shown that it is possible to use a winter and spring series of SAR images to determine

[15] Surface roughness is another primary factor that influences the strength of a radar signal return.
[16] Here I am referring to moisture content as being water in a liquid state. Frozen and gaseous water respond differently to microwave energy than liquid water.
[17] Subsurface features can induce a modulation in surface of a body of water, somewhat like the way a swell of water in a fast moving stream marks the location of a submerge boulder. SAR can be used to detect this surface expression of subsurface features (Mouchot and Garello, 1998).

relative lake depth based on the extent to which the lake water freezes to the lake bottom (Sellmann et al, 1975; Elachi and Bryan 1976; Mellor, 1982; Jeffries et al, 1996).

Figure 22. Radarsat SAR composite image of the Iditarod River study area. The areas that were dry in July but wet in September show up as the red areas around the perimeter of the more circular bog-formed lakes and near the ends of the oxbow lakes.

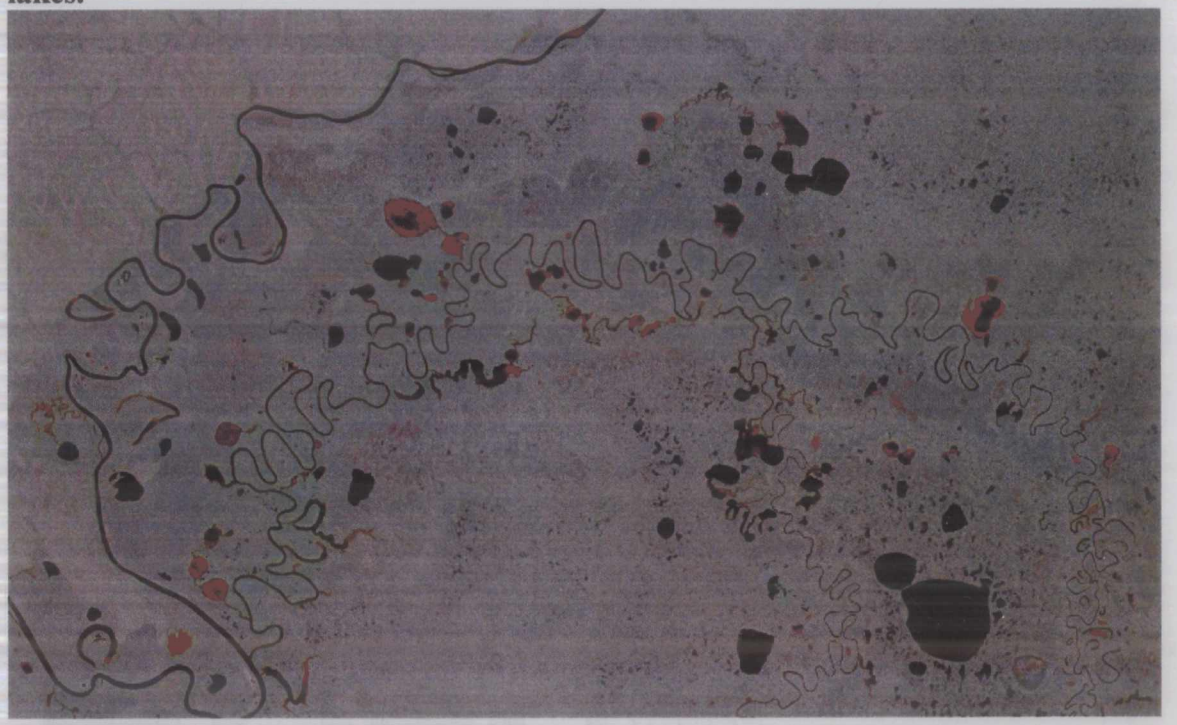

4.2.2 Salix alaxensis

There are several reasons why the delineation of S. alaxensis was unsuccessful. The technique used to detect S. alaxensis relied primarily on the ability to use satellite imagery to detect sandbars. Initially, multitemporal, georeferenced SAR imagery was used, but because Innoko River is U-shaped, small changes in water level do not result in large changes in the area of exposed sandbar. Increasing the resolution of the imagery – for example using Radarsat's fine beam mode (8 meter nominal resolution) – does not necessarily make the sandbars any easier to distinguish. The positional error associated with each image (at normal and low water levels) further complicates the problem of isolating these narrow individual sandbars using multitemporal SAR imagery (Figure 23).

Figure 23. Positional error associated with mulit-temporal imagery complicates the task of delineating sandbars.

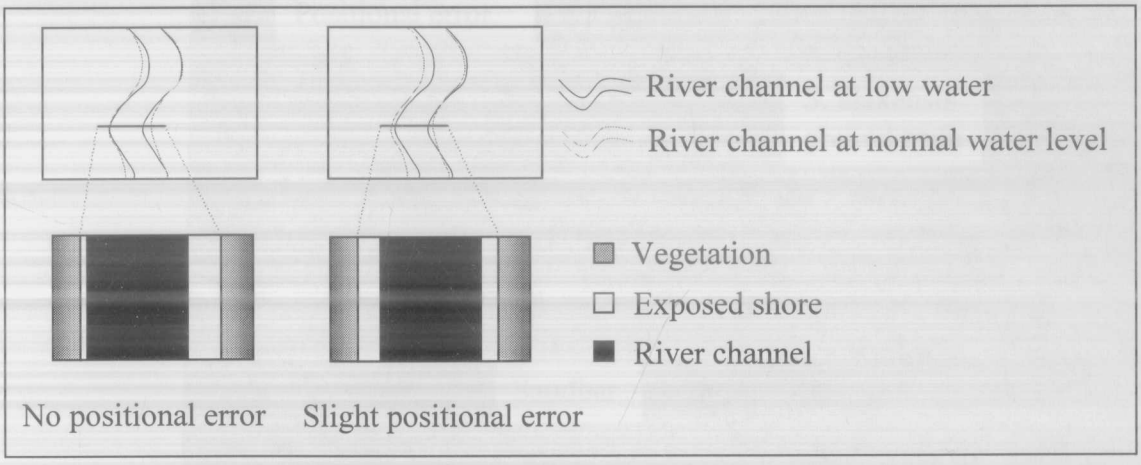

Fortunately, it is also possible to detect sandbars using Landsat ETM+ imagery. However, there are some drawbacks. ETM+ does not possess the same all weather capability as SAR, and therefore obtaining a cloud free image on a date when the river is at its lowest (and therefore the most sandbars are exposed) is much more difficult.

Unlike lakes there is no clear boundary that marks a stand of *S. alaxensis*, especially in the part of the stand that marks the transition between S. alaxensis and the lowland forest which consists mainly of other broadleaf species such as balsam poplar,

paper birch, and alder with scattered white spruce trees. This can complicate the process of collecting ground truth. Additionally, it was evident from the ground truth that S. alaxensis grows well beyond the immediate vicinity of the sandbars. In fact, it stretches for quite a distance along the river in an ever-narrowing band (Figure 24). This, and the positional error associated with satellite data (both GPS coordinates and imagery) complicate the task of using the spectral reflectance to delineate *S. alaxensis.*

Figure 24. *Salix alaxensis* grows beyond the immediate vicinity of the sandbars. Positional error associated with both the imagery and the ground truth makes it difficult to know exactly where *S. alaxensis* occurs (S. alaxensis is marked by polygons with crosshatching).

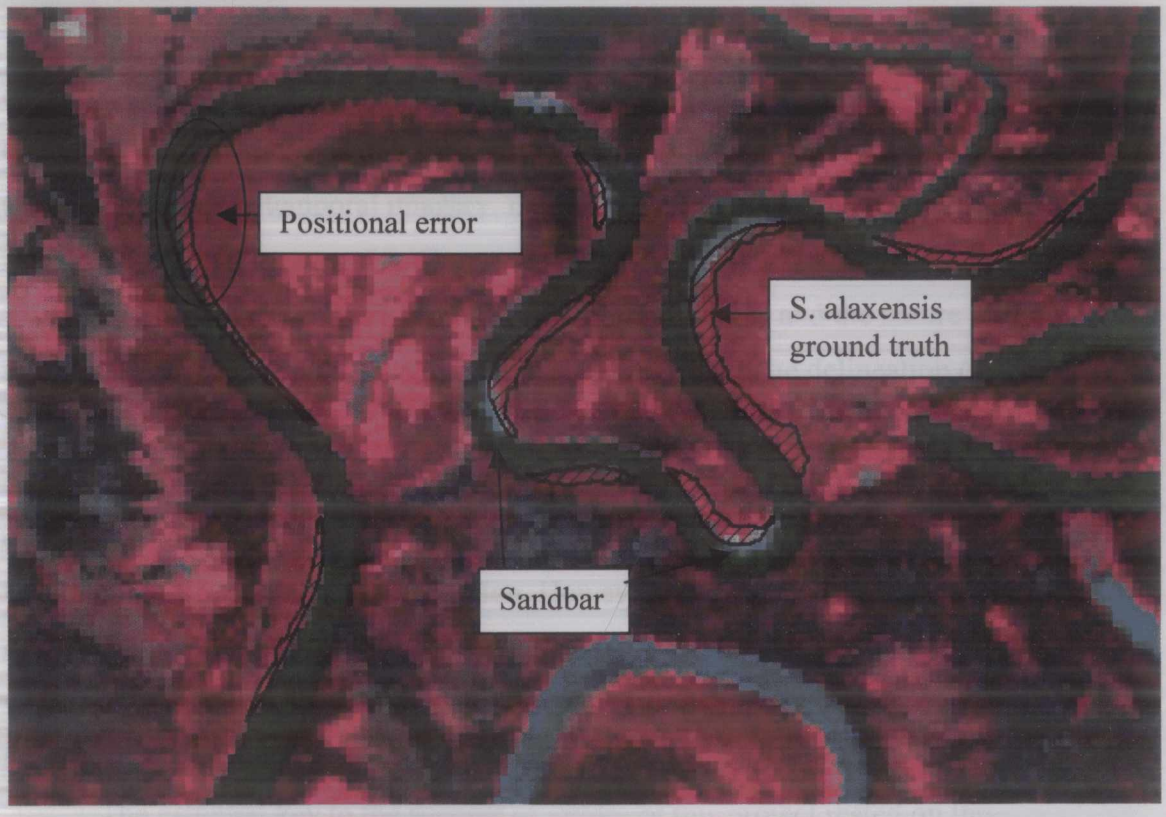

CHAPTER 5. CONCLUSIONS AND RECOMMENDATIONS

5.1 Conclusions

The objective of this study was to evaluate the effectiveness of georeferenced Landsat ETM+ and multitemporal SAR imagery to:

1. Delineate draw down lakes in the vicinity of the Iditarod River.
2. Delineate S. alaxensis along the Innoko River corridor and

While this study met with mixed results, one must keep in mind that it focused on a very limited area. There still remains the potential for land planners to apply the techniques used in this study to aid their decision-making efforts.

Multitemporal, georeferenced Radarsat SAR imagery proved to be useful for detecting draw down lakes in the Iditarod River region, yielding an estimated overall classification accuracy of 78%. The dynamic nature of draw down lakes makes them easy to detect using multitemporal imagery. Large changes in their surface extent can be easily monitored through the use of SAR.

Because of the growth characteristics of *S. alaxensis* and the nature of the Innoko River it was not feasible to use the same technique used in the delineation of draw down lakes to delineate sandbars and therefore *S. alaxensis*. This was clearly evident in estimated accuracies presented in Tables 4 and 5 from section 4.2.1. Based on the results of this study an estimated 98% of S. alaxensis occurs within 120 meters of the river and within 30 meters of broadleaf vegetation. However, of all of the areas that meet those two requirements, only an estimated 9% was actually *S. alaxensis*. While it is easy to know where S. alaxensis grows, it is difficult to separate it from the other broadleaf vegetation that shares a similar habitat along the river corridor.

The essential key to the success or failure of this project rested on the circumstances surrounding the element that I was trying to delineate. Lakes were easy to delineate because a small change in water level resulted in a large change in the surface extent of the draw down lakes and it was possible to minimize the effects of positional error. For the detection of *S. alaxensis*, the positional error associated with satellite data

and the u-shape nature of the Innoko River[18] contributed to make it impractical to use multitemporal SAR or Landsat ETM+ to delineate sandbars, and therefore, potentially *S. alaxensis*.

5.2 Recommendations

One question that arose as a result of this study was whether or not the classification of draw down lakes could be improved by taking into account method of lake formation and therefore the shape and bathymetry of the lake. Did the difference in bathymetry and total surface area of round bog-formed lakes make them draw down differently than oxbow lakes? To answer this question you must first be able to separate the round bog lakes from the more linear oxbow lakes. One approach is to calculate a dimensionless ratio using the lakes area and perimeter as shown in equation 5. Lakes that are round will have a ratio that approaches 1. Lakes that are more linearly shaped will have a ratio of less than one.

$$\frac{area}{\frac{(perimeter)^2}{4\pi}} \tag{5}$$

Because no lake is perfectly round, the ratio for every lake will be less than that of a perfect circle, but how much less depends on whether or not the lake is round or shaped linearly. Unfortunately, the Iditarod River study area had too few draw down oxbow lakes to develop a model that would test this theory.

One possible method of improving the delineation *S. alaxensis* would be to develop a rigorous statistical model that predicts the distribution of *S. alaxensis* based on georeferenced satellite imagery and site information (e.g. elevation, slope, aspect, distance to water) from known locations of *S. alaxensis* and their surrounding areas. This would essentially increase the number of criteria that a location would have to meet before it could be classified as *S. alaxensis* and it would include information from the surrounding area into the model development.

[18] The u-shape means that a small change in water level will not result in a large change in the area of exposed sandbar.

Another possible method of delineating *S. alaxensis* is to use low altitude aerial photography. Since *Salix alaxensis* occurs exclusively within the immediate vicinity of the river much time and money could be saved by limiting the data acquisition to the river corridor.

Delineating an individual species such as *S. alaxensis* is an intriguing problem, especially in such a remote location. It is difficult to devise methods that circumvent the confounding effects of positional error, both from satellite imagery and from GPS coordinates.

LITERATURE CITED

Alt, K.T. 1983. Inventory and Cataloging of Sport Fish and Sport Fish Waters of Western Alaska. Alaska Department of Fish and Game. Federal Aid in Fish Restoration Project F-9-15, Study Number G-1, Volume 24:34-71.

Anderson, J.R., E.E. Hardy, J.T. Roach, and R.E. Witmer. 1976. A Land Use and Land Cover Classification System for Use with Remote Sensor Data. U.S. Geological Survey professional paper No. 964. Washington, D.C.

Bishop, Y.M.M, S.E. Fienberg and P.W. Holland. 1975. Discrete Multivariate Analysis: Theory and Practice. MIT Press, Cambridge, MA. 557 pp.

Campbell, J.B. 1996. Introduction to Remote Sensing. The Guilford Press, New York, NY. 622 pp.

Congalton, R.G. and K. Green. 1998. Assessing the Accuracy of Remotely Sensed Data: Principles and Practices. Lewis Publishers, Boca Raton, FL. 137 pp.

Congalton R.G. 1991. A Review of Assessing the Accuracy of Classifications of Remotely Sensed Data. Remote Sensing of Environment. 37:35-46.

Cibula, W.G. and M.O. Nyquist. 1987. Use of Topographic and Climatological Models in a Geographical Data Base to Improve Landsat MSS Classification for Olympic National Park. Photogrammatic Engineering and Remote Sensing. 53(1):67-75.

Drury, S.A. 1998. Images of the Earth: A Guide to Remote Sensing. Oxford University Press, New York, NY. 203 pp.

Elachi, C. and M.L. Bryan. 1976. Imaging Radar Observations of Frozen Arctic Lakes. Remote Sensing of Environment. 5:169-175.

Ely, C.R and A.X. Dzubin. 1994. Greater White-fronted Goose (Anser albifrons). In The Birds of North America, No 131 (A. Poole and F.Gill, Eds.). Philadelphia: the Academy of Natural Sciences; Washington, D.C.: The American Ornithologists' Union.

Eyre, F.H. (ed). 1980. Forest Cover Types of the United States and Canada. The Society of American Foresters, Washington, D.C. 148 pp.

Henderson, F.M. and A.J. Lewis (eds.) 1998. Principles and Applications of Imaging RADAR, third edition. John Wiley and Sons, New York, NY. 866 pp.

Hess, L.L., J.M. Melack, S. Filoso, and Y. Wang. 1995. Delineation of Inundated Area and Vegetation Along the Amazon Floodplain with the SIR-C Synthetic Aperture Radar. IEEE Transactions on Geoscience and Remote Sensing. 33(4):896-904.

Hudson, M.S. 1983. Waterfowl Production on Three Age-Classes of Stock Ponds in Montana. Journal of Wildlife Mangement. 47(1):112-117.

Ioka, M. and M. Koda. 1986. Performance of Landsat-5 TM Data in Land-cover Classification. International Journal of Remote Sensing. 7(12):1715-1728.

Jeffries, M.O., K. Morris, and G.E. Liston. 1996. A Method to Determine Lake Depth and Water Availability on the North Slope of Alaska with Spaceborne Imaging Radar and Numerical Ice Growth Modeling. Arctic. 49(4):367-374.

Janssen, L.L.F., M.N. Jaarsma, and E.T.M. van der Linden. 1990. Integrating Topographic Data with Remote Sensing for Land Cover Classification. Photogrammetric Engineering and Remote Sensing. 56(11):1503-1506.

Jensen, J.R., and D.C. Cowan. 1999. Remote Sensing of Urban/Suburban Infrastructure and Socio-Economic Attributes. Photogrammatic Engineering and Remote Sensing. 65(5): 611-622.

Kasischke, E.S., J.M. Melack, and M.C. Dobson. 1997. The Use of Imaging Radars for Ecological Applications – A Review. Remote Sensing of Environment. 59:141-156.

Lee, J.S., I. Jurkevich, P. Dewaele, P. Wambacq, and A. Oosterlinck. 1994. Speckle Filtering of Synthetic Aperture Radar Images: A Review. Remote Sensing Reviews. 8:313-340.

Lee, J.S. and I. Jurkevich. 1989. Segmentation of SAR Images. IEEE Transactions in Geoscience and Remote Sensing. 27(6):674-680

Lewis, A.J., F.M. Henderson, and D.W. Holcomb. 1998. Radar Fundamentals: the Geoscience Perspective. In: Principles and Applications of Imaging RADAR, third edition. John Wiley and Sons, New York, NY. 131-181 pp.

Lillesand, T.M., and R.W. Kiefer. 2000. Remote Sensing and Image Interpretation. John Wiley and Sons, Inc. New York, NY.

Mellor, J.C. 1982. Bathymetry of Alaskan Arctic Lakes: a Key to Resource Inventory with Remote Sensing Methods, Ph.D. Dissertation, University of Alaska, Fairbanks, AK.

Michelson, D.B., B.M. Liljeberg, and P. Pilesjö. 2000. Comparison of Algorithms for Classifying Swedish Landcover Using Landsat TM and ERS-1 SAR. Remote Sensing of Environment. 71:1-15.

Milne, A.K., G. Horn, and M. Finlayson. 2000. Monitoring Wetlands Inundation Patterns using RADARSAT Mulittemporal Data. Canadian Journal of Remote Sensing. 26(2):133-141.

Mouchot, M.C., and R. Garello. 1998. SAR for Oceanography. In: Principles and Applications of Imaging RADAR, third edition. John Wiley and Sons, New York, NY. 631-675 pp.

Nezry, E., E. Mougin, A. Lopes, J.P. Gastellu-Etchegorry. 1993. Tropical Vegetation Mapping with Combined Visible and SAR Spaceborne Data. International Journal of Remote Sensing. 14(11):2165-2184.

NOAA. 1984. Visual Interpretation of TM Band Combinations Being Studied. Landsat Data User Notes, No. 30. pp 7-9.

Pielou, E. C. 1994. A Naturalist's Guide to the Arctic. The University of Chicago Press, Chicago, MA. pp 327.

Pope, K.O., E. Rejmankova, J.F. Paris, and R. Woodruff. 1997. Detecting Seasonal Flooding Cycles in Marshes of the Yucatan Peninsula with SIR-C Polarimetric Radar Imagery. Remote Sensing of Environment. 59:157-166.

Quattrochi, D. A. and R. E. Pelletier. 1991. Remote Sensing for Analysis of Landscapes: An Introduction. In: Quantitative Methods in Landscape Ecology. M. G. Turner and R. H. Garder eds. Springer-Verlag, New York, NY. 51-76 pp.

Ranson, K.J., and G. Sun. 1994. Northern Forest Classification Using Temporal Multifrequency and Multipolarimetric SAR Images. Remote Sensing of Environment. 47:142-153.

Raney, R.K. 1998. Radar Fundamentals: Technical Perspective. In: Principles and Applications of Imaging RADAR, third edition. John Wiley and Sons, New York, NY. 9-130 pp.

Risenhoover, K.L. 1989. Composition and Quality of Moose Winter Diets in Interior Alaska. Journal of Wildlife Management. 53(3):568-577.

Sabins, F.F. 1997. Remote Sensing: Principles and Interpretation, third edition. W.H. Freeman and Co. New York. 494 pp.

Schriever, J.R. and R.G. Congalton. 1995. Evaluating Seasonal Variability as an Aid to Cover-Type Mapping from Landsat Thematic Mapper Data in the Northeast. Photogrammetric Engineering and Remote Sensing. 61(3):321-327.

Selkregg, L.L., ed. 1976. Alaska Regional Profiles Yukon Region. University of Alaska, Fairbanks. Arctic Environmental Information Data Center, Ancorage, AK. Vol 6. 346 pp.

Sellmann, P.V, W.F. Weeks and W.J. Campbell. 1975. Use of Side-Looking Airborne Radar to Determine Lake Depth on the Alaskan North Slope. US Army Cold Regions Research and Engineering Laboratory, Hanover, NH, SR 230.

Skidmore, A.K. 1999. Accuracy Assessment of Spatial Information. In: Spatial Statistics for Remote Sensing. A. Stein, F. Van der Meer and B. Gorte, eds. Kluwer Academic Publishers. Dordrecht, The Netherlands. 197-209 pp.

Skinner, B., W. Erickson, L. McDonald, and J. Minick. 1996. Moose winter range capacity: a progress report. Innoko National Wildlife Refuge, McGrath, AK. 25 pp.

Swanson, G.A. 1988. Aquatic Habitats of Breeding Waterfowl. In: The Ecology and Management of Wetlands, Volume I: Ecology of Wetlands. D.D. Hook, W.H. McKee, Jr., H.K. Smith, J. Gregory, V.G. Burrell, Jr., M.R. DeVoe, R.E. Sojka, S. Gilbert, R. Banks, L.H. Stolzy, C. Brooks, T.D. Matthews and T.H. Shear, eds. Timber Press, Portland Oregon. 195-202 pp.

Talbot, S.S., and C.J. Markon. 1987. Landsat-assisted vegetation mapping of Innoko National Wildlife Refuge, Alaska. In: 5th Scandinavian Conference on Image Analysis. J.Eklundh, ed. International Association for Pattern Recognition, Stockholm, Sweden. 269-277 pp.

USFWS. 1987. Innoko National Wildlife Refuge, Comprehensive Conservation Plan, Environmental Impact Statement, Wilderness Review. USFWS, Anchorage, AK. 255 pp.

Verbyla, D.L. 1995. Satellite Remote Sensing of Natural Resources. CRC Press, Inc. New
York, NY. 198 pp.

Viereck, L.A. and E.L. Little. 1972. Alaska Trees and Shrubs. USDA FS. Agricultural Handbook No. 410, Washington D.C. 256 pp.

Wang, J., J. Shang, B. Brisco, and R.J. Brown. 1998. Evaluation of Mulit-date ERS-1 and Multispectral Landsat Imagery for Wetland Detection in Southern Ontario. Canadian Journal of Remote Sensing. 24(1):60-68.

Waring, R.H, J. Way, E. R. Hunt Jr., L. Morrissey, K.J. Ranson, J.F. Weishampel, R. Oren and S.E. Franklin. 1995. Imaging Radar for Ecosystem Studies. BioScience. 45(10):715-723.

Weast, R.C., M.J. Astle, and W.H. Beyer (eds). 1984. The CRC Handbook of Chemistry and Physics. CRC Press. Boca Raton, FL.

Wolter, P.T., D.J. Mladenoff, G.E. Host, and T.R. Crow. 1995. Improved Forest Classification in the Northern Lake States Using Multi-Temporal Landsat Imagery. Photogrammetric Engineering and Remote Sensing. 61(9):1129-1143.

PERSONAL COMMUNICATION

Linne, Mitch. U.S. Fish and Wildlife Service, Division of Water Resources. Anchorage, Alaska.

Platte, Bob. U.S. Fish and Wildlife Service, Division of Migratory Bird Management. Anchorage, Alaska.

APPENDICIES

APPENDIX A. Sensor and orbital characteristics of satellites used in this study.

Table 6. Landsat 5 TM orbital characteristics and spectral bands (Adapted from Sabins, 1997 and Quattrochi and Pelletier, 1991).

Band	Bandwidth (μm)	Color	Spatial Resolution (m)	Radiometric Resolution (bits)	Primary Use
1	0.45-0.52	Blue-green	30x30	8	Shallow bathymetry, distinguishing soil vs. veg. & deciduous vs. coniferous
2	0.52-0.6	Green	30x30	8	Designed to measure green reflectance peak of vegetation
3	0.63-0.69	Red	30x30	8	Discrimination of veg. types
4	0.76-0.90	Reflected IR	30x30	8	Biomass content and mapping shorelines, determining vegetation types, and soil moisture discrimination
5	1.55-1.75	Reflected IR	30x30	8	Useful for differentiating snow from clouds.
6	10.4-12.5	Thermal IR	60x60	8	Nighttime images, soil moisture
7	2.08-2.35	Reflected IR	30x30	8	Geological mapping and vegetation moisture content

Altitude –705 km
Swath width – 185x172 km
Repeat cycle – 16 days
Crosses 40° N latitude –10:30am
Orbits per day – 14.5
Number of orbits (paths) – 233
Image sidelap at equator – 7.6%

Table 7. Landsat 7 ETM+ orbital characteristics and spectral bands (Adapted from http://ltpwww.gsfc.nasa.gov/IAS/handbook/handbook_htmls/chapter5/chapter5.html and Sabins, 1997)

Band	Bandwidth (μm)	Color	Spatial Resolution (m)	Radiometric Resolution (bits)	Primary Use
1	0.45-0.52	Blue-green	30x30	8	Shallow bathymetry, soil vs. vegetation & decid. vs. conif. discrimination
2	0.52-0.6	Green	30x30	8	Designed to measure green reflectance peak of vegetation
3	0.63-0.69	Red	30x30	8	Discrimination of veg. types
4	0.76-0.90	Reflected IR	30x30	8	Vegetation biomass content and mapping shorelines, determining vegetation types, and soil moisture discrimination
5	1.55-1.75	Reflected IR	30x30	8	Useful for differentiating snow from clouds.
6	10.4-12.5	Thermal IR	60x60	8	Night images, soil moisture
7	2.08-2.35	Reflected IR	30x30	8	Geological mapping and vegetation moisture content
8	0.5-0.9	Pan-chromatic	15x15	8	Higher resolution veg. mapping

Swath width – 183x170 km **Orbits per day** – 14 **Altitude** –705 km
Repeat cycle – 16 days **Number of orbits (paths)** – 233
Image sidelap at equator – 7.3% **Descending equatorial crossing time** – 10:00am

Table 8. Sensor and orbital characteristics of RADARSAT SAR (http://www.space.gc.ca/csa_sectors/earth_environment/radarsat/radarsat_info/description/specifications.asp)

Frequency / Wavelength	5.3GHz/C-band 5.6 cm
RF Bandwidth	11.6, 17.3 or 30.0 Mhz
Transmitter Power (peak)	5 kW
Transmitter Power (average)	300 W
Maximum Data Rate	85 Mb/s (recorded) - 105 Mb/s (R/T)
Antenna Size	15m x 1.5m
Antenna Polarization	HH
Launch mass (total)	2,750 kg
Array power	2.5 kW
Batteries	3 x 48 Ah NiCd
Design Lifetime	5 years
Altitude	793-821 kilometers
Inclination	98.6 degrees
Period	101 minutes
Ascending node	18:00 hours
Sun-synchronous	14 orbits per day

Table 9. RADARSAT SAR imaging modes (http://www.space.gc.ca/csa_sectors/earth_environment/radarsat/radarsat_info/description/specifications.asp).

Mode	**Nominal Resolution (m)**	**# of Positions/ Beams**	**Swath Width (km)**	**Incidence Angles (degrees)**
Fine	8	15	45	37-47
Standard	30	7	100	20-49
Wide	30	3	150	20-45
ScanSAR Narrow	50	2	300	20-49
ScanSAR Wide	100	2	500	20-49
Extended (H)	18-27	3	75	52-58
Extended (L)	30	1	170	10-22

APPENDIX B. A land use/land cover classification system for remote sensor data.

Table 10. Land use and land cover classification system for use with remote sensor data (Anderson et al, 1976).

Level I	Level II
1 Urban or Built-up Land	11 Residential.
	12 Commercial and Services.
	13 Industrial.
	14 Transportation, Communications, and Utilities.
	15 Industrial and Commercial Complexes.
	16 Mixed Urban or Built-up Land.
	17 Other Urban or Built-up Land.
2 Agricultural Land	21 Cropland and Pasture.
	22 Orchards, Groves, Vineyards, Nurseries, and Ornamental Horticultural Areas.
	23 Confined Feeding Operations.
	24 Other Agricultural Land.
3 Rangeland	31 Herbaceous Rangeland.
	32 Shrub and Brush Rangeland.
	33 Mixed Rangeland.
4 Forest Land	41 Deciduous Forest Land.
	42 Evergreen Forest Land.
	43 Mixed Forest Land.
5 Water	51 Streams and Canals.
	52 Lakes.
	53 Reservoirs.
	54 Bays and Estuaries.

Table 10. Continued.

6 Wetland	61 Forested Wetland.
	62 Non-forested Wetland.
7 Barren Land	71 Dry Salt Flats.
	72 Beaches.
	73 Sandy Areas other than Beaches.
	74 Bare Exposed Rock.
	75 Strip Mines, Quarries, and Gravel Pits.
	76 Transitional Areas.
	77 Mixed Barren Land.
8 Tundra	81 Shrub and Brush Tundra.
	82 Herbaceous Tundra.
	83 Bare Ground Tundra.
	84 Wet Tundra.
	85 Mixed Tundra.
9 Perennial Snow or Ice	91 Perennial Snowfields.
	92 Glaciers.

APPENDIX C. Land cover classes and acreage of the Innoko NWR.

Table 11. Acreage summary of land cover classes on Innoko Refuge (Talbot, 1987; USFWS, 1987)

Land Cover Class	Federal (acres)	Private (acres)	Percent Total Refuge
FOREST CLASSES			
Closed Needleleaf Forest	285,030	30,341	8.3
Open Needleleaf Forest	488,750	24,770	13.5
Needleleaf Woodland	81,930	7,450	2.3
Mixed Forest	129,690	36,930	4.4
SCRUB CLASSES			
Broadleaf/Tall Scrub	319,520	54,650	9.8
Lowland/Tall Scrub	230,130	14,410	6.4
Subalpine Scrub	3,140	1,380	0.1
Prostrate Dwarf Shrub Tundra	50	0	0.0
Erect Dwarf Shrub Heath (subalpine)	300	80	0.0
WETLAND CLASSES			
Dwarf Shrub-Graminoid Tussock Peatland	327,830	26,990	9.3
Dwarf Shrub-Graminoid Peatland (Flat Bog)	337,010	13,110	9.1
Raised Bog with Scattered Trees	311.010	7,250	8.3
Alluvial-Graminoid Marsh	61,300	1,870	1.6
Shrub-Graminoid Marsh	434,650	16,300	11.8
Graminoid Bog	20,560	10	5.4
Graminoid Tussock Dwarf Shrub Peatland	118,380	4,890	3.2
Scarcely Vegetated Floodplain	310	560	0.0

Table 11. Continued.

MISCELLANEOUS CLASSES			
Upland Burn Regeneration	273,910	17,830	7.7
Scarcely Vegetated Scree	310	0	0.0
WATER CLASSES			
Clear Water	111,490	9,890	3.2
Sedimented Water	1,970	1,850	0.2

APPENDIX D. Acquisition dates and registration errors for images in this study.

Table 12. List of acquisition dates, and registration errors for images used in this study.

Sensor	Image ID #	Date of Acquisition	Pixel Dimensions (meters)	# of links used in registration	Model RMS error (pixels)
Landsat 7	L71075016_01619990630 L71075015_01519990630	06/30/1999	30	65	0.3407
Radarsat	R1_13929_ST6_159	07/06/1998 (1)	12.5	33	0.4856
Radarsat	R1_13929_ST6_158	07/06/1998 (2)	12.5	37	0.4752
Radarsat	R1_14951_ST6_291	09/15/1998 (1)	12.5	41	0.4838
Radarsat	R1_14951_ST6_293	09/15/1998 (2)	12.5	40	0.4851

APPENDIX E. Ground control point information.

Figure 25. Ground control points used to check the registration accuracy of the Landsat 5 TM image.

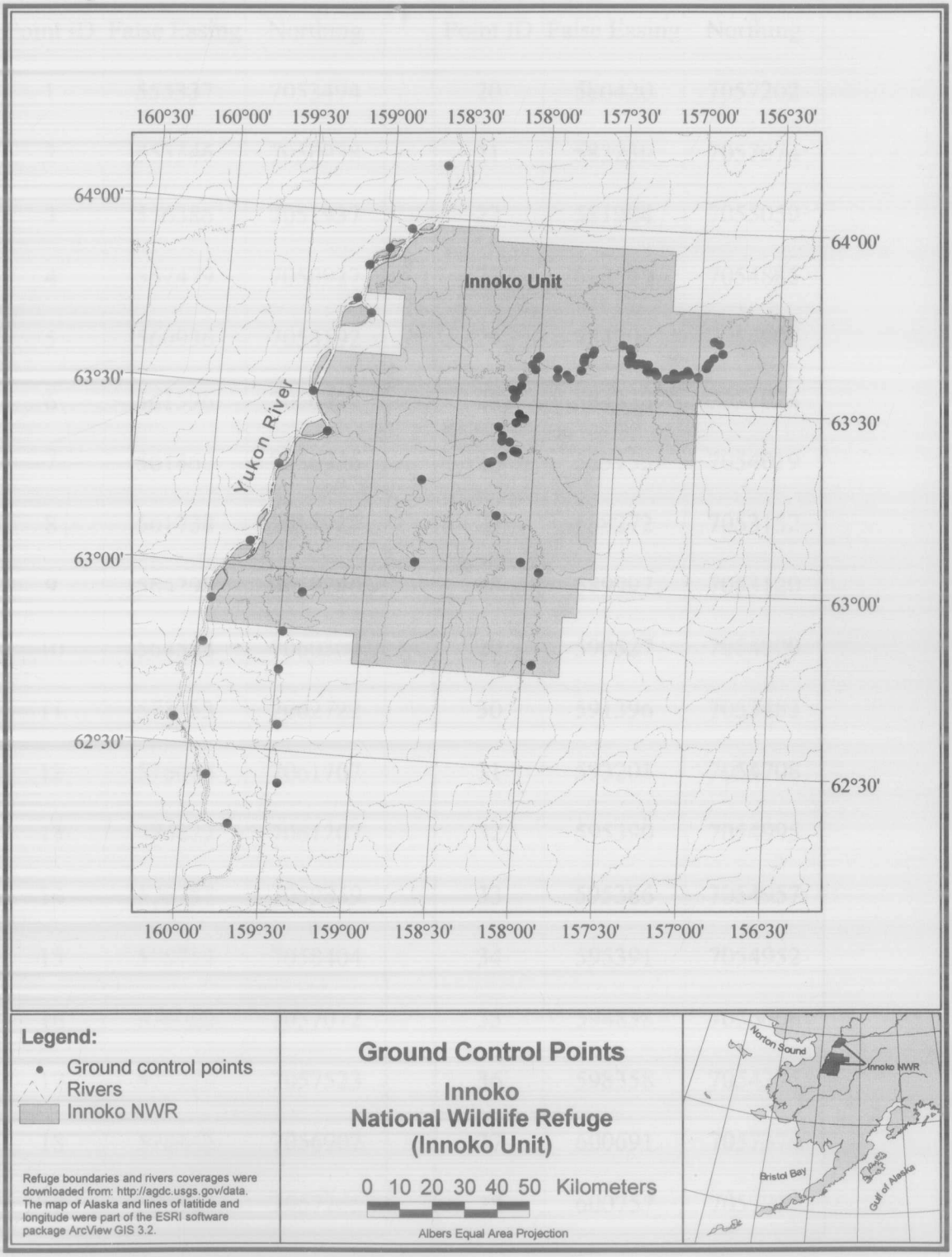

Table 13. Ground control point coordinates. Coordinates are in Universal Transverse Mercator Projection (UTM) Zone 4, North American Datum 1927 (NAD27).

Point ID	False Easing	Northing
1	553337	7053494
2	553346	7050938
3	556386	7051937
4	557479	7050927
5	560936	7053592
6	561596	7056497
7	561460	7056976
8	561738	7057917
9	564298	7059246
10	564588	7060304
11	573753	7062722
12	576088	7061707
13	576222	7061207
14	576757	7059849
15	575712	7058404
16	576060	7057072
17	577221	7057523
18	578445	7056902
19	578994	7057265

Point ID	False Easing	Northing
20	580420	7057202
21	582230	7057074
22	581984	7055059
23	582529	7054885
24	584201	7054907
25	584378	7055024
26	585155	7054019
27	588272	7053152
28	589997	7053120
29	590527	7054900
30	591396	7053483
31	593201	7054708
32	595390	7054995
33	595386	7054957
34	595391	7054952
35	594838	7056008
36	598358	7054375
37	600691	7057374
38	600757	7057779

Table 13. Continued.

39	601183	7058638
40	601481	7059048
41	602876	7060733
42	605605	7062308
43	604467	7065244
44	602691	7065933
45	547209	7057155
46	546447	7056435
47	546166	7052953
48	545043	7054438
49	542128	7049902
50	542069	7047450
51	539381	7045986
52	540006	7045732
53	540868	7045627
54	540304	7043645
55	540206	7043417
56	542061	7038324
57	543765	7036991
58	541218	7035514
59	535610	7033736
60	537134	7031054
61	537075	7029389
62	539540	7029207
63	542303	7026086
64	541992	7026100
65	541647	7026232
66	541198	7026339
67	537592	7024492
68	534377	7022517
69	533376	7022140
70	496409	7088334
71	487150	7071606
72	491901	7067150
73	475006	7040956
74	480591	7028411
75	465603	7016947
76	458307	6991656
77	447153	6972635
78	476280	6976459

Table 13. Continued.

79	511799	6988790
80	445476	6958449
81	437751	6933895
82	449496	6916099
83	457698	6900861
84	472648	6914928
85	471335	6933658
86	470405	6951343
87	470875	6963548
88	513112	7115979
89	503071	7095036
90	490256	7082470
91	546028	6991184
92	551963	6958460
93	552071	6988247
94	536970	7005444
95	512090	7015183

Figure 26. Location of draw down lakes and non draw down lakes for the Iditarod River study area.

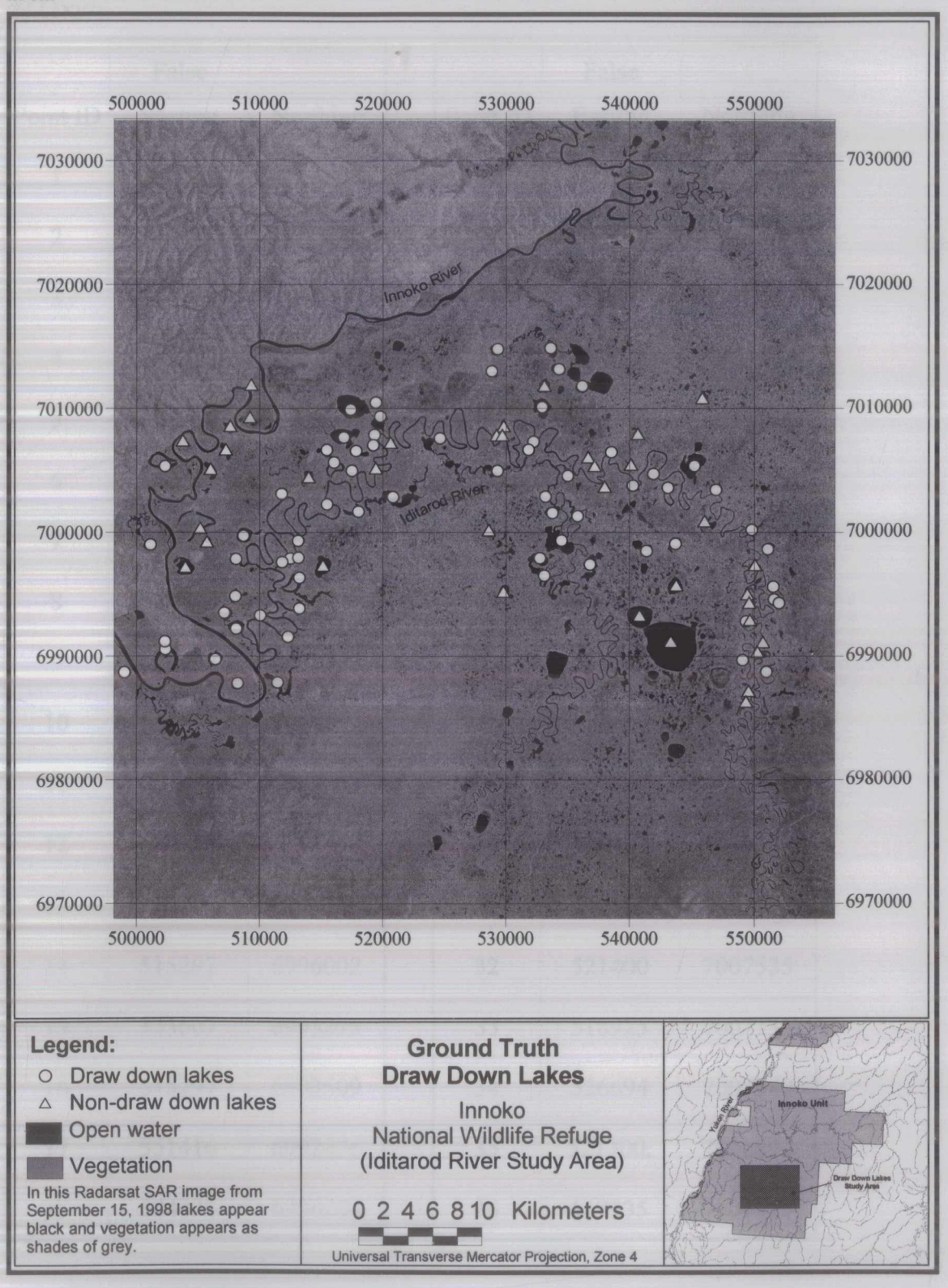

Table 14. Ground truth coordinates of draw down lakes. Coordinates are in Universal Transverse Mercator (UTM) Zone 4, North American Datum 1927 (NAD27).

Point ID	False Easting	Northing
1	534297	7006976
2	540613	7006140
3	518122	7005309
4	504382	7004998.5
5	531362	7004625.5
6	545119	7003277.5
7	548978	7003093
8	522886	7002520.5
9	520098	7001339
10	537870	7000952
11	551859	6999861
12	514559	6997553
13	513894	6997258
14	515297	6996002
15	553607	6995275
16	515297	6993509
17	551416	6992476
18	504421	6990204

Point ID	False Easting	Northing
19	551133	6989349
20	553048	6988404
21	513525	6987527
22	535688	7014540
23	531388	7014458
24	536348	7012849
25	530914	7012684
26	511515	7011773
27	538256	7011478
28	521503	7010153
29	534997	7009766
30	519462	7009592
31	521869	7009005
32	521400	7007535
33	518925	7007335
34	526694	7007240
35	521300.	7006692
36	517535	7006325

Table 14. Continued.

37	533891	7006314
38	519913	7006248
39	547242	7005046
40	543963	7004383
41	537064	7004208
42	542319	7003433
43	513854	7002759
44	535255	7002533
45	517556	7001922
46	535819	7001213
47	510753	6999383
48	536560	6999003
49	515186	6998983
50	545740	6998751
51	503210	6998673
52	553172	6998314
53	543427	6998158
54	515217	6997608
55	534825	6997564
56	510141	6997514
57	538874	6997060
58	535166	6996156
59	510098	6994499
60	509197	6993163
61	512113	6992951
64	504371	6990847
65	508472	6989398
66	501101	6988355
67	510293	6987471

Table 15. Ground truth coordinates of non draw down lakes. Coordinates are in Universal Transverse Mercator (UTM) Zone 4, North American Datum 1927 (NAD27).

Point ID	False Easting	Northing
1	517223	6997021
2	508088	7004810
3	509317	7006391
4	506038	6996904
5	511393	7011633
6	509669	7008273
7	505840	7007107
8	511271	7008987
9	507250	7000039
10	507790	6998930
11	516057	7004162
12	522701	7006935
13	548076	7000604
14	531881	7008247
15	531302	7007517
16	531759	7007517
17	538731	7005751
18	539249	7005051

Point ID	False Easting	Northing
19	540071	7003376
20	542719	7007638
21	542171	7005172
22	552127	6997074
23	551518	6994699
24	551679	6994013
25	551740	6992635
26	552785	6990831
27	552346	6990043
28	551634	6986892
29	551422	6986013
30	545389	6990888
31	542886	6992974
32	545807	6995426
33	531882	6994904
34	535168	7011540
35	547893	7010549
36	521504	7004865

Table 15. Continued.

37	530683	6999858

Figure 27. Ground truth locations for Salix alaxensis in the Innoko River study area.

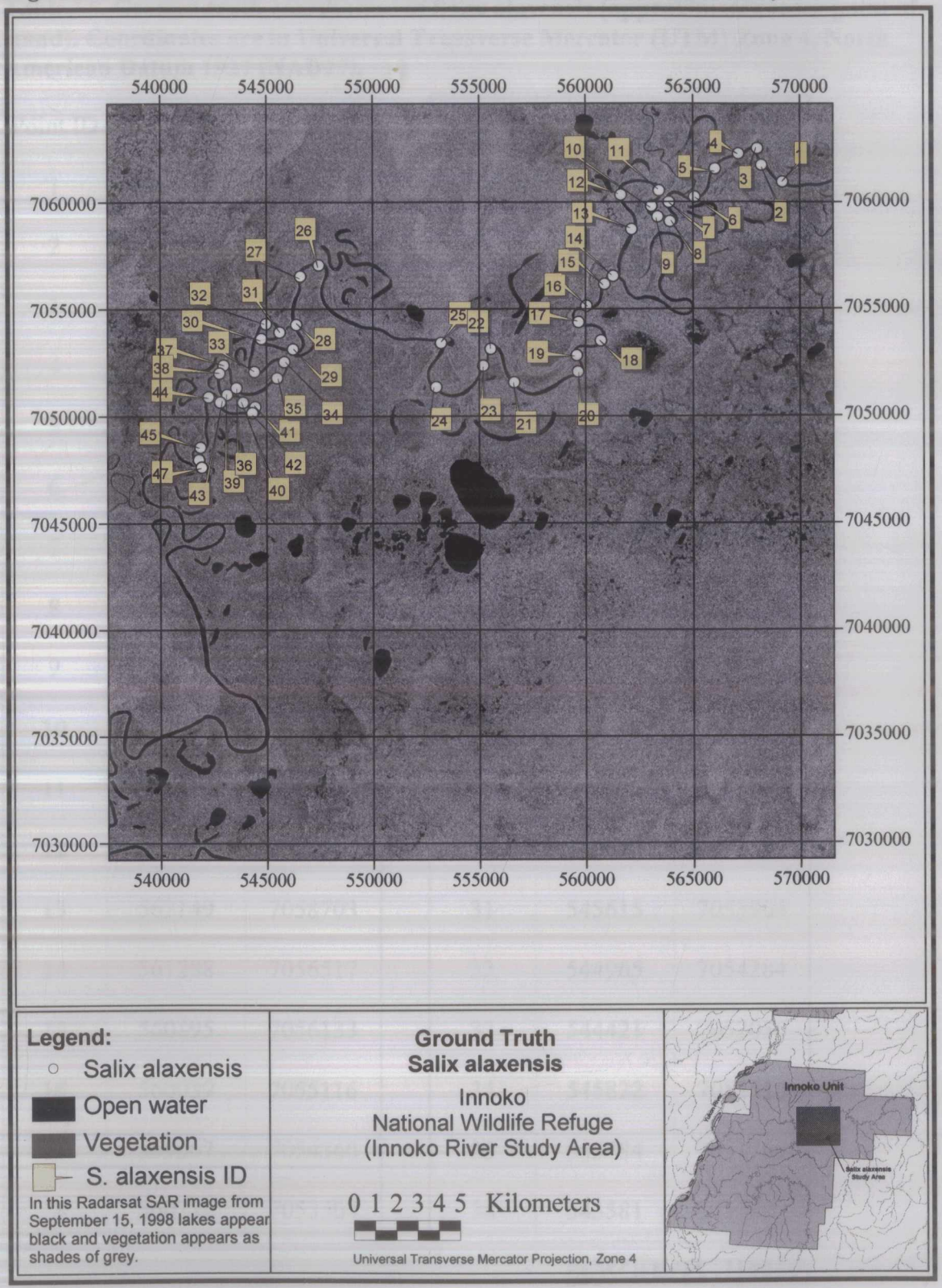

Table 16. Ground truth coordinates of Salix alaxensis (approximate center point of stand). Coordinates are in Universal Transverse Mercator (UTM) Zone 4, North American Datum 1927 (NAD27).

Point ID	False Easing	Northing
1	569166	7060922
2	568192	7061711
3	568002	7062496
4	567107	7062243
5	566027	7061521
6	565069	7060205
7	563883	7059969
8	563929	7059074
9	563364	7059289
10	563073	7059787
11	563419	7060513
12	561655	7060310
13	562149	7058703
14	561288	7056517
15	560895	7056133
16	560039	7055116
17	559667	7054360
18	560722	7053504

Point ID	False Easing	Northing
19	559587	7052807
20	559638	7052052
21	556642	7051554
22	555532	7053111
23	555182	7052326
24	552970	7051335
25	553202	7053385
26	547467	7057023
27	546594	7056500
28	546391	7054255
29	546235	7053107
30	544746	7053592
31	545615	7053904
32	544965	7054284
33	544421	7052056
34	545822	7052516
35	545484	7051769
36	543581	7051309

Table 16. Continued

37	542969	7052364
38	542771	7051984
39	543134	7050993
40	543885	7050634
41	544454	7050423
42	544328	7050144
43	542809	7050647
44	542268	7050883
45	541884	7048532
46	541804	7047950
47	541939	7047608

APPENDIX F. Data used to develop the criteria in the lake classification system.

Table 17. Data used in the calculation of percent change of lake surface area between the dates of July 6, 1998 and September 15, 1998 for non draw down lakes.

False Easing	Northing	Area - Sept. 15, 1998 (normal water levels) (ha)	Area - July 6, 1998 (low water levels) (ha)	% change
506038	6996904	136.41	139.50	2.27
508088	7004810	70.05	73.17	4.46
511271	7008987	17.06	16.67	-2.29
516057	7004162	60.03	60.47	0.73
517224	6997021	149.52	149.23	-0.19
530683	6999858	20.67	20.25	-2.04
531883	6994904	63.69	63.80	0.17
540071	7003376	6.64	7.55	13.65
542720	7007638	18.81	19.14	1.74
547893	7010549	47.34	49.55	4.65
551422	6986013	3.84	4.52	17.48
551634	6986892	6.66	5.95	-10.56
507924	7000870	82.39	42.53	-48.38

Mean % change in surface area = -1.408 (n=13, s =15.75)

Table 18. Data used in the calculation of percent change of lake surface area between the dates of July 6, 1998 and September 15, 1998 for draw down lakes.

False Easing	Northing	Area - Sept. 15, 1998 (normal water levels) (ha)	Area - July 6, 1998 (low water levels) (ha)	% change
504382	7004999	84.98	67.56	-20.50
509197	6993163	72.59	5.05	-93.05
510293	6987471	49.44	49.13	-0.63
513855	7002759	12.31	2.34	-80.96
515187	6998983	9.64	0.77	-92.06
515218	6997608	21.84	18.30	-16.24
519463	7009593	361.69	53.53	-85.20
521401	7007536	7.27	6.08	-16.34
521870	7009005	100.19	6.59	-93.42
526695	7007240	281.69	127.03	-54.90
530914	7012685	38.81	26.63	-31.40
533891	7006314	19.11	10.64	-44.32
536348	7012850	48.56	47.83	-1.51
537871	7000952	32.98	12.92	-60.82
547243	7005046	255.88	110.95	-56.64
548978	7003093	13.33	5.55	-58.38
551417	6992476	1.02	1.17	15.39
553048	6988404	3.78	4.23	11.98
553173	6998314	53.58	3.31	-93.82

Table 18. Continued.

553608	6995275	6.53	5.34	-18.18

Mean % change in surface area = -44.55 (n = 20, s = 37.50)

APPENDIX G. Lake data.

Table 19. Data used to assign lakes to either the 'draw down' or 'non draw down' class (excluding lakes used in the model development).

False Easting	Northing	Area during normal water levels (ha)	Area during low water levels (ha)	% change	Lake type[19]
551134	6989349	2.00	2.52	25.78	dd
504372	6990847	32.08	32.17	0.29	dd
545119	7003278	27.28	26.92	-1.32	dd
543963	7004383	4.16	4.06	-2.26	dd
535256	7002533	10.09	9.64	-4.49	dd
538256	7011478	591.44	546.50	-7.60	dd
518925	7007336	216.86	194.52	-10.30	dd
535819	7001213	52.27	46.77	-10.52	dd
504422	6990205	116.39	100.13	-13.98	dd
535689	7014541	57.25	47.86	-16.40	dd
534826	6997564	157.09	128.44	-18.24	dd
535167	6996156	117.67	95.80	-18.59	dd
510141	6997514	65.41	51.42	-21.38	dd
534998	7009767	160.11	125.50	-21.62	dd
536561	6999003	299.45	234.30	-21.76	dd
518123	7005309	111.36	84.34	-24.26	dd

[19] ndd = non draw down, dd = draw down. It should be noted that lake type information is part of the ground truth information. It was not determined by the % change in surface area of the lake.

Table 19. Continued.

538874	6997060	141.63	106.30	-24.95	dd
520099	7001339	44.27	30.53	-31.03	dd
522887	7002521	304.17	209.08	-31.26	dd
542320	7003433	3.06	2.06	-32.65	dd
534297	7006976	3.64	2.44	-33.05	dd
537065	7004208	30.72	20.39	-33.62	dd
521504	7010153	42.16	27.45	-34.88	dd
501101	6988355	20.17	13.00	-35.55	dd
515298	6996003	145.33	92.64	-36.25	dd
512114	6992951	5.27	3.08	-41.54	dd
513525	6987527	124.34	71.50	-42.50	dd
531389	7014458	70.05	39.58	-43.50	dd
503210	6998673	124.77	68.56	-45.05	dd
510099	6994499	71.47	39.08	-45.32	dd
515298	6993510	44.63	22.75	-49.02	dd
545741	6998751	18.38	8.55	-53.49	dd
521301	7006692	24.50	9.64	-60.65	dd
543427	6998158	81.72	32.00	-60.84	dd
519913	7006248	33.00	12.14	-63.21	dd
514376	6991218	2.59	0.86	-66.87	dd
513894	6997258	13.06	2.97	-77.27	dd

Table 19. Continued.

540614	7006140	5.09	1.13	-77.91	dd
551859	6999862	13.47	2.83	-79.00	dd
514559	6997554	7.91	1.06	-86.56	dd
510169	6991872	116.30	4.48	-96.14	dd
510754	6999383	111.19	3.14	-97.18	dd
508472	6989398	81.59	0.00	-100.00	dd
517556	7001922	1.55	0.00	-100.00	dd
551680	6994013	7.33	7.83	6.82	ndd
538731	7005751	5.41	5.58	3.18	ndd
531759	7007517	6.19	6.36	2.78	ndd
539249	7005051	7.50	7.63	1.67	ndd
548076	7000604	36.17	36.66	1.34	ndd
545807	6995426	114.59	116.13	1.34	ndd
509318	7006391	49.56	50.17	1.23	ndd
531303	7007517	11.38	11.50	1.10	ndd
542172	7005172	6.81	6.84	0.46	ndd
535168	7011540	71.84	71.91	0.09	ndd
545390	6990888	1343.02	1343.09	0.01	ndd
531881	7008247	39.95	39.86	-0.24	ndd
542887	6992974	279.59	278.83	-0.27	ndd
507791	6998930	32.52	32.38	-0.43	ndd

Table 19. Continued.

552347	6990043	10.38	8.55	-17.62	ndd
551518	6994699	13.70	7.78	-43.22	ndd
551740	6992635	2.34	1.27	-46.00	ndd
552786	6990831	2.39	1.17	-50.98	ndd
521504	7004865	13.77	6.08	-55.85	ndd